MHD research, inc.

POST OFFICE BOX 1815, NEWPORT BEACH, CALIFORNIA

RESEARCH ON THE PHYSICS OF CONTINUOUS AND PULSED MHD GENERATORS

SEMIANNUAL TECHNICAL SUMMARY REPORT

By: Malcolm S. Jones
R. C. Brumfield
E. Evans
C. McKinnon
T. Naff
C. Rockman
C. Snyder

Advanced Research Projects Agency

Nonr-3859(00)

Project Code 9800

Order No. 099-370 3-27-62 (Amend. #4)

February 1963

RESEARCH ON THE PHYSICS OF CONTINUOUS AND PULSED MHD GENERATORS

by

Malcolm S. Jones, Jr.
Robert C. Brumfield
Earl Evans
Charles McKinnon
Thomas Naff
Charles Rockman
Calvin Snyder

FIRST SEMI-ANNUAL TECHNICAL REPORT
Contract Nonr 3859(00)
1 June 1962 to 31 December 1962

Advanced Research Projects Agency
Order No. 209-62/11-16-61 (Amend. #4)
Project Code 9800

February 1963

This work has been sponsored by the Advanced Research Projects Agency through the Power Branch of the Office of Naval Research. Reproduction in whole or in part is permitted for any purpose of the U. S. Government.

RESEARCH ON THE PHYSICS OF CONTINUOUS AND PULSED MHD GENERATORS

ABSTRACT

Short duration electrical pulses of 1.8 MW peak power have been produced from 10 grams of seeded condensed explosives by MHD principles. The pulse length is about 10 microseconds. Low ionization potential materials are applied either as surface seeding or mixed into the bulk explosive. The effect upon power output of the geometry of the explosion tube, the size, geometry and composition of the explosive charge, and magnetic field intensity and electrode geometry are discussed.

Longer duration pulsed power in the time range of one millisecond to one second will be produced using non-detonating (deflagrating) explosives. This apparatus is described, and various potential seeded propellants are discussed.

Numerical calculations and microwave probing experiments of seeded combustion product flows indicate that electron attachment in combustion product gases may be an important factor in determining conductivity.

Various scaling and geometry considerations for several configurations of explosive-driven MHD generators are discussed.

TABLE OF CONTENTS

RESEARCH ON THE PHYSICS OF CONTINUOUS AND PULSED MHD GENERATORS

1. INTRODUCTION AND SUMMARY

1.1 Introduction

One of the most attractive features of MHD power generation is the potential for achieving very high specific power outputs from small sized, light weight devices. With the present day techniques, power outputs of the order of 10^{10} watts per cubic meter appear achievable. By comparison the output of Hoover Dam is approximately 10^{9} watts. There are many applications in which electrical power at these levels is used for a fraction of a second, with a fairly long interval between use periods. Examples of systems which use power in pulses of this type are high power radar sets, sonar systems, X-ray sources, etc. Other possible systems which might require similar pulses of power are laser light pumps, magnetic metal forming devices, and emergency communication systems. It was with this type of requirement in mind that a program was undertaken to produce large pulses of electrical power by MHD principles.

1.2 Summary

The work reported herein covers the continuation and extension of work carried out under contract Nonr 3523(00). It is primarily an experimental program in which various methods for producing large pulses of power for short times by MHD principles have been investigated. The time regimes under study cover the period between 1 and 100 microseconds, although steps are being taken to extend the times of interest to periods of about 1 second. In general, the experiments are conducted in times short compared to the thermal time constants of materials so that thermal ablation of walls and electrodes is not important, and there is no need for forced convection cooling.

The initial experimental work has been carried out using condensed explosives which have been seeded with low ionization potential materials. This work is described in detail in Section 2 of this report. Power outputs of the order of 1.8 MW have been achieved in a volume of about one cubic inch, which is equivalent to a power density of 10^{11} watts per cubic meter. Pulse lengths are approximately 5 to 10 microseconds, and can be controlled by the geometry of the experiment. Extensive work has indicated that the power is extracted from the seeded detonation product gases, rather than from the shock front which is driven by the explosive. Some initial studies of the problem associated with scaling this type of generator to larger sizes are presented in Appendix I. This study indicates that the explosive-driven pulsed MHD generator will probably be competitive with other methods of pulsed power generation such as capacitor banks or inductors.

In order to extend the time scale of the experiments, a program has been started which will use seeded deflagrating explosives, or propellants. A number of possible chemical systems have been examined analytically. It is indicated that systems which burn a metal with cesium nitrate should produce a high conductivity reactant flow stream suitable for MHD channel experiments. The experimental apparatus is described in Section 3 along with a discussion of potentially useful propellant systems. This experiment will be in operation during the first quarter of 1963.

At the conclusion of contract Nonr 3523(00) a number of topics associated with negative ion formation in combustion product MHD channel flow were left in a state of partial completion. This previous work was reported in detail in Reference 1. Numercial calculations and microwave attenuation measurements, reported in Section 4, indicate that negative ion formation in a buffering gas is an

important process, but that previous machine calculations had over-estimated the effect. No further work is planned in this area.

2. PULSED POWER FROM SHAPED EXPLOSIVES

2.1 Introduction

The purpose of this portion of the program has been the investigation of methods for the production of pulses of electrical power from condensed explosives by MHD principles. Pulse power sources of the explosion tube type have potential advantages of simplicity, compactness, portability, convenience, reliability, and storability. The use of various types and geometric forms of chemical explosive sources can make possible operation at various power levels (one KW to thousands of MW) and for variable periods of time, (1 microsecond up to 1 millisecond).

In the present experiments the electrical output characteristics from a seeded shaped charge detonated in the explosion tube have been studied. The hot partially ionized combustion gases from the detonation, pass at high velocity through the power generation section. In the MHD generator section, the electric power is generated by the relative motion of the ionized gas through a transverse magnetic field. The electrical current is extracted by means of copper electrodes connected to an external load. Work on this phase of the project was initiated on 10 June 1962 and the first experimental run was made on 16 August 1962.

There are a large number of factors which must be investigated in order to establish applicable design criteria for explosive-driven generators which will allow intelligent scaling from the present small scale experiment. These include: the geometry of the explosive tube, the size, geometry, and composition of the explosive charge, the type, fractional composition, and location of the low ionization potential seed materials, and the effects of magnetic field intensity and electrode geometry upon power output.

It was with this comprehensive list of topics to be investigated in mind that the experimental facilities were designed and constructed. To date only a portion of the above-mentioned factors have been studied and the following discussion will present the results of this work.

2.2 Description of the Apparatus

The experimental apparatus used for the experiments consists of five basic parts as shown in the schematic of Figures 2.1 and 2.2. These are: (1) explosion tube or driver section, (2) the MHD channel or test section, (3) diagnostic instrumentation, (4) electromagnet, and (5) evacuated dump tube and tank. Figure 2.3 is a photograph of the complete facility; Figure 2.4 is a photograph of the interior of the generator.

The explosion tube is a stainless steel cylinder 2.25 inches inside diameter, 0.5 inch wall and 6 inches long. The tube shown in Figure 2.4 has contained approximately 50 explosive shots. The noticeable bulge of the tube is caused by the high peak pressure load on each detonation which causes an increase in diameter of about 0.006 inches for each shot. Most of the explosive energy, about 90%, goes into deformation of the confining chamber. Only a small fraction of the energy, at present of the order of 1%, goes into the high-speed jet which is produced by the shaped charge. The explosive driver, the black object in Figure 2.4 just below the explosion tube, is a 10 gram commercial shaped charge (duPont Model 20B jet perforator). The explosive in the jet perforator is generally a waxed RDX (cyclotrimethylene-trinitramine) composition. The copper liner of the perforator is removed prior to firing the charge. Firing is initiated by an electric blasting cap which sets off the explosive primacord, shown attached to the bottom of the shaped charge. The primacor serves as

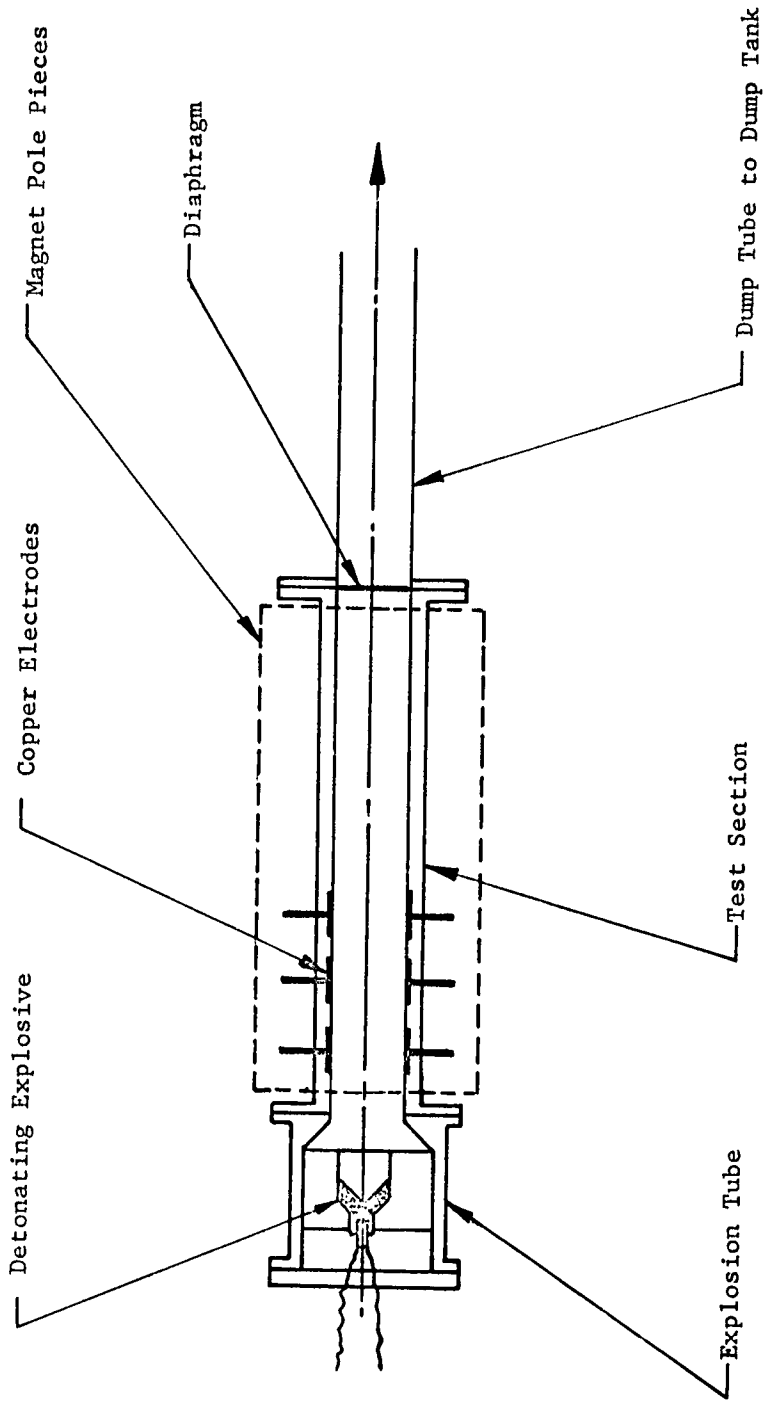

Figure 2.1 Schematic Diagram of Experimental Apparatus

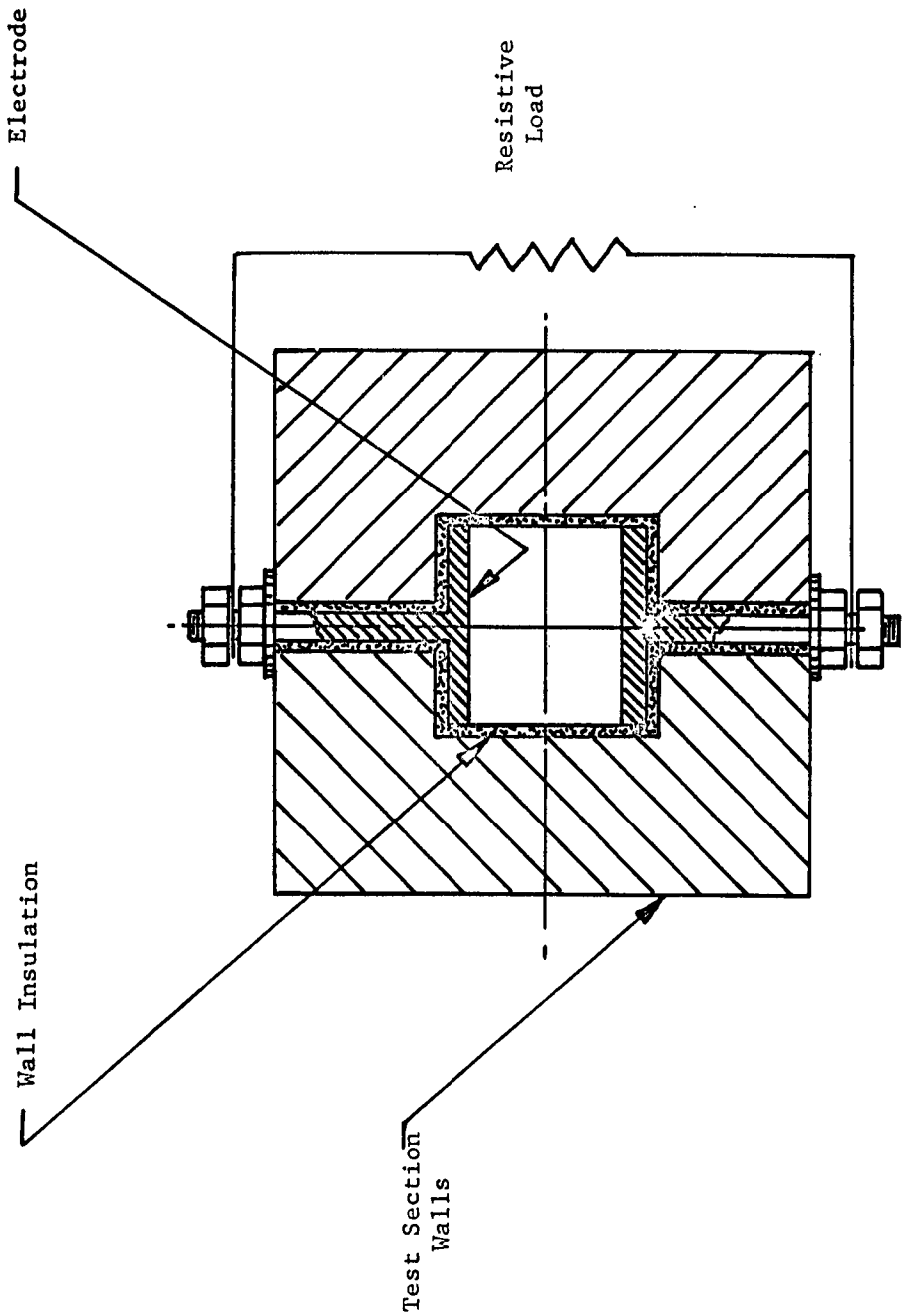

Figure 2.2 Section View of Test Section Showing One Electrode Pair

Figure 2.3 Photograph of the overall facility.

Figure 2.4 Photograph showing the disassembled generator.

an explosive train to carry the detonation to the booster at the base of the RDX charge. The explosive is seeded with a low ionization potential compound (cesium picrate) in a fashion which is described in a subsequent section. The charge is held in the center of the explosion tube by a polystyrene spacer, the white cylindrical object to the right of the shaped charge in Figure 2.4.

The driven section, or MHD generator proper, is a square steel channel of one-inch inside dimension and 18 inches long. The walls of the test section are 0.75 inch thick. The top and bottom spacer bars which hold the electrodes are of stainless steel; the channel sidewalls are made of soft magnetic steel. The purpose of soft steel is to reduce the width of the gap in the magnet. With a lower reluctance, a given power source can produce a higher magnetic field in the test section. The inside walls of the channel are insulated with fiber reinforced phenolic strips (micarta). The test section is fitted with copper electrodes which are flush with the inside walls and whose centers are spaced two inches apart down the channel. The electrodes are unheated copper, 1.00 inch wide, but of varying lengths in the flow direction . Electrodes have been studied with the following lengths in the flow direction: 0.25 inch, 0.50 inch, and 2.00 inches. The short electrodes shown in Figure 2.4 are 0.25 inch long. The space between the electrodes is filled with phenolic strips to maintain a smooth contour.

Readout of data thus far has been accomplished with Tektronix 551 dual-beam oscilloscopes equipped with Polaroid cameras. A small triggering electrode situated at the explosion end of the test section uses the v x B voltage developed by the jet to trigger the oscilloscope inputs. Resistive loads are fastened across the electrode pairs on the outside of the channel as is indicated schematically in Figure 2.2. The resistive loads pass through the slots milled into the outside of the side plates (shown in Figure 2.4) so as to provide minimum inductance path.

The test section has been operated with air at atmospheric pressure in the channel for the majority of the experiments; however, provision has been made for the partial evacuation of the test section by means of a vacuum pump. The cylindrical dump tank and muffler at the left side of Figure 2.3 is also evacuated by the vacuum pump. The exit from the test section into the tank is sealed with a Mylar diaphragm which is ruptured by the explosive jet. The dump tank is employed strictly in order to muffle the noise produced by the explosive charge.

The magnet shown was formerly used in combustion powered MHD generation experiments. Magnetic fields of 22 kilogauss can be produced across the one-inch channel with the present power supply, which is a 50 KW motor generator set.

2.3 Electrical Measurements

The measurements performed to date have been of two types: (1) measurements of the induced voltage across the resistive load between the electrode, and (2) measurements of the elapsed time between arrival of the conductive gases at different stations down the channel. Both types of measurements are derived from the oscilloscope traces for the various electrode pairs down the channel. Figure 2.5 is a set of typical oscilloscope traces showing the output voltage for a half-inch long electrode, which was mounted at a station four inches from the entrance to the generator. The three traces shown are for three separate values of load resistance: 1070 ohms for trace A, 0.44 ohms for trace B, and 0.005 ohms for trace C. Each trace was taken on a separate shot with sweep speed and vertical gain as noted. The value of the load resistor was changed and the channel cleaned out between each shot. The output voltage, aside from the inductive effects, is proportional to the current. The output voltage rises rapidly, about 12 microseconds after the trigger signal, reaching a peak value in a few microseconds. The duration of the pulse and rate at which the

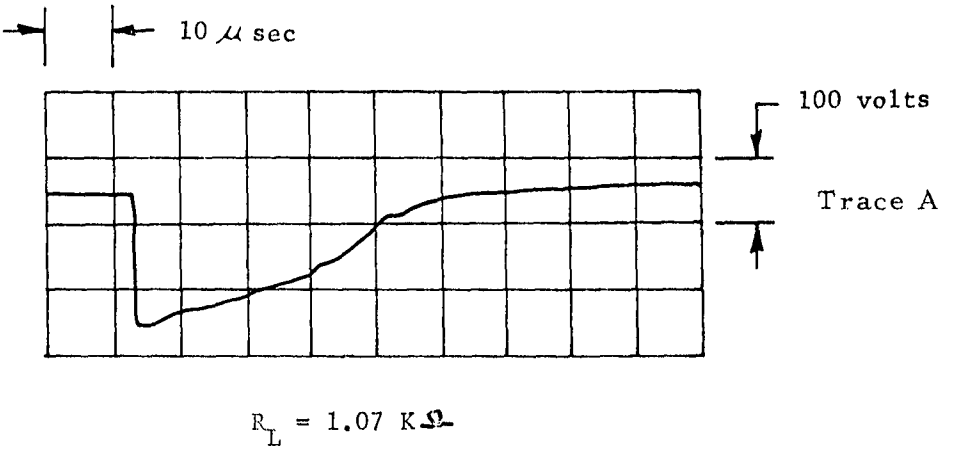

R_L = 1.07 KΩ

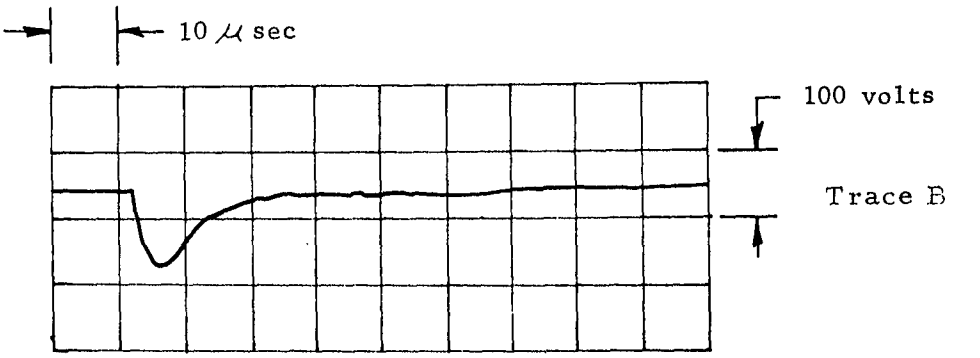

R_L = 0.44 Ω

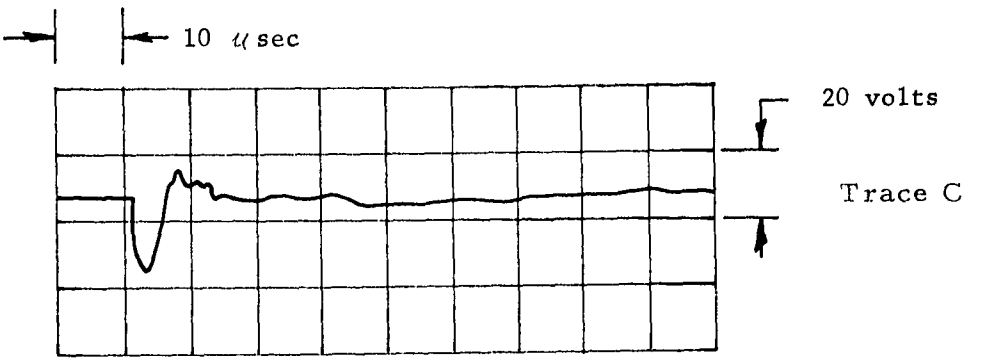

R_L = 0.005 Ω

Figure 2.5 Three typical oscilloscope traces showing the output voltage as a function of load resistance for 0.5 inch long electrode.

current decays depends upon the value of the load impedance. For high impedance loads, trace A, the current continues for about 50 microseconds; for the intermediate case, trace B, the current persists for about 20 microseconds; whereas, for the low impedance load, the current lasts for only 5 or 6 microseconds. The negative output voltage, after the initial positive peak (trace C) is believed due to inductive effects.

Since the voltage across a load resistor is what is experimentally determined, the power being generated is equal to the square of this output voltage, divided by the value of the load resistance. The peak power generated in trace A is about 40 W, in trace B about 20 KW, and in trace C about 90 KW. These three traces clearly indicate that the majority of the power being generated comes from the first few centimeters of the slug of seeded detonation products which is flowing down the channel. Trace A indicates that the flow of conductive materials lasts for about 50 microseconds, or longer. However, after a few microseconds the internal impedance of the channel becomes very high so that the output voltage drops almost to zero for the low impedance loads. The internal impedance of the generator can be determined from voltage-current plots, which will be discussed in a following section.

Need for Seed Material. In early experiments it was quickly noted that it was necessary to seed the explosive in order to produce appreciable amounts of power from the generator. In a typical set of experiments with a magnetic field of 15 kilogauss, an unseeded 10 gram charge produced an open circuit voltage of approximately 130 volts, and the approximate internal impedance of the generator as determined from the voltage-current plot, was about 150 ohms. The maximum indicated power level, assuming a linear voltage-current relationship was 28 watts. When the 10 gram charges were surface seeded with 0.2 grams of cesium carbonate, the open circuit

voltage increased to 230 volts, the generator had an internal impedance 0.5 ohms, and the peak power output was approximately 74 KW. It should be noted that the use of cesium seed material resulted in a factor of 300 reduction in generator internal impedance. In subsequent experiments using other seed methods (surface seeding with cesium picrate, an "active" seed), much higher power levels were achieved.

Analysis of the data indicated that some power is being produced from the explosive-driven air shock (the unseeded case discussed above). However, the power which can be generated from the air shock is relatively insignificant, of the order of 10% or less, in comparison to the power which can be produced from the seeded detonation products.

Electrodes. A variety of different electrode configurations have been used. For most of the experiments the currents were measured for 4 electrode pairs, 2 inches apart. As a subordinate experiment, the output of one electrode located at different positions in the channel has also been investigated. The electrodes have been of the three lengths cited, 0.25 inch, 0.50 inch, and 2.00 inches, all 1.00 inch wide. One-half inch diameter round electrodes have also been used. The electrode resistor load has been varied from open circuit (20 megohms) to nearly short circuit (2 milliohms). The majority of the experiments have been carried out with the same resistive load on all electrodes down the channel. The load resistors have been fabricated from short lengths of copper wire for the milliohm sizes.

Various methods of grounding have been used to connect the electrodes to the oscilloscopes. These have been either with the cathodes grounded, the anode grounded, or with the cathode and anode electrodes at floating potential with respect to ground, i.e., un-

grounded. The method of grounding did not make any appreciable difference in the power output. However, a negative precurser pulse, which is sometimes present, disappears when the oscilloscopes are operated ungrounded.

Conductivity. Figures 2.6, 2.7, and 2.8 are peak voltage-peak current plots for three different sized electrodes located at different distances down the channel. The voltage-current (V-I) plots are derived from scope traces for various values of the load resistor. The peak output voltage, V, is the ordinate, with the peak current, I = V/R, as the abscissa. All of the data plotted in these figures are for electrodes 1.00 inch wide. The electrodes for Figures 2.6 were 0.25 inches long, for Figure 2.7 they were 0.50 inches long, and for Figure 2.8 they were 2.00 inches long.

It can be seen that the current-voltage curves are strongly non-linear indicating an arc type conduction at high currents. There are apparently two modes of operation. For high values of load resistance and current less than a few hundred amperes the V-I curve is approximately linear. The internal impedance of the first electrode in the generator, derived from the linear portion of the V-I curve leads to a value of conductivity of approximately 800 mhos/meter. The conductivity decays in an approximate exponential fashion with distance downstream with a characteristic length of approximately 10 cm.

At a current density of approximately 200 to 300 amperes per cm^2, the current-voltage characteristic becomes non-linear. Low values of load impedance lead to very large currents which require low sustaining voltages, similar to an electric arc. The apparent impedance of the generator in the arc mode is an order of magnitude less than in the linear mode. The highest current measured thus far in the arc mode is 18,000 amperes. It is believed that the non-linear conductivity may be due to either boundary layer effects or non-linear effects in the

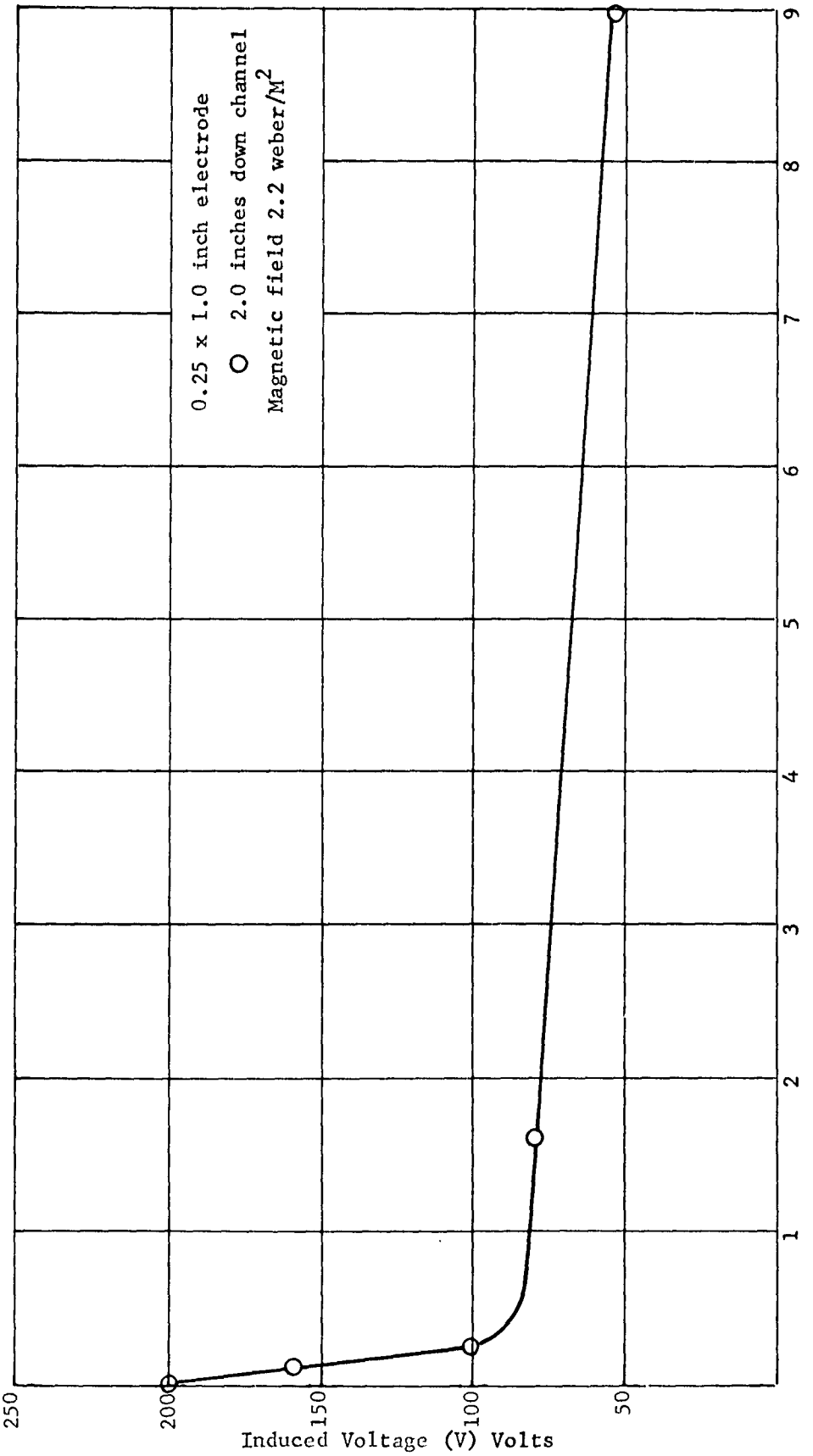

Figure 2.6 Values of peak voltage and peak current for 0.25 inch x 1.00 inch electrode. Center of electrod is located 2.0 inches from entrance to channel.

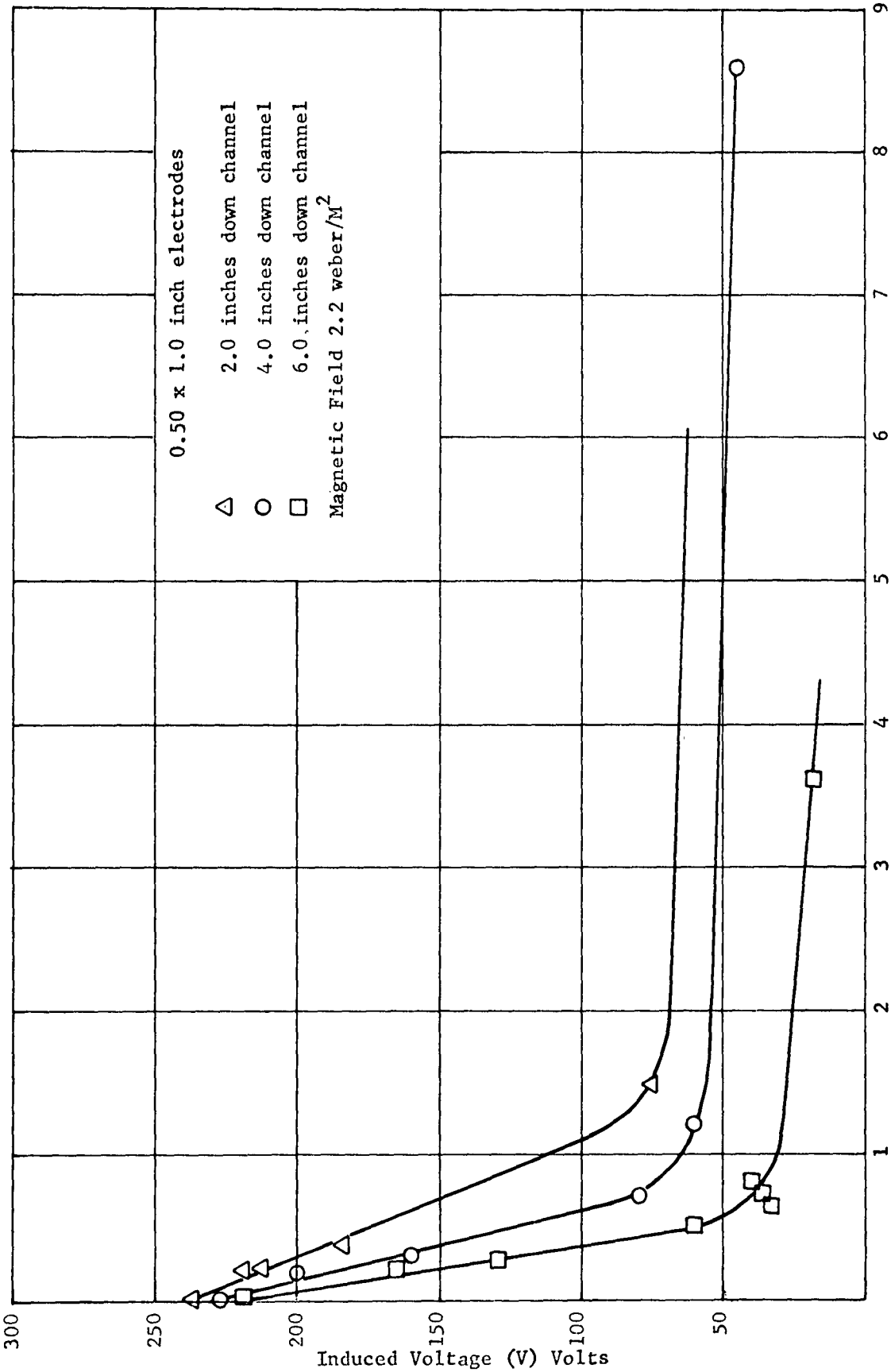

Figure 2.7 Values of peak voltage and peak current for 0.50 inch electrodes. Centers of electrodes are located 2.0, 4.0, and 6.0 inches from the channel entrance.

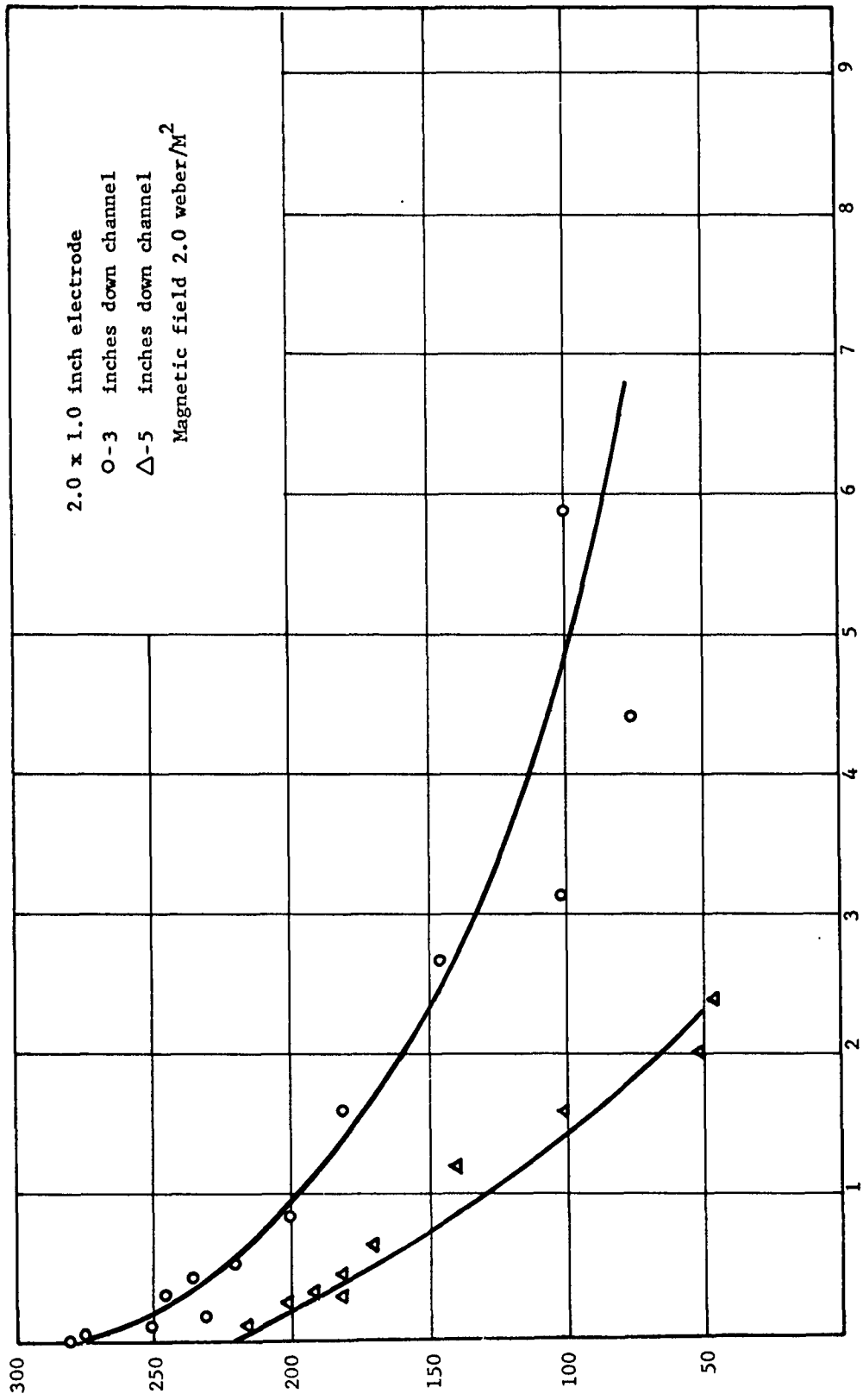

Figure 2.8 Values of peak voltage and peak current for 2.00 inch electrodes. Centers of electrodes are located 4.0 and 6.0 inches from channel entrance.

gas. A similar effect has been observed by Nagamatsu[2]. Thus far, it has not been possible to fully explore the consequences of this non-linear current relationship, however, in the next report period the measurements will be extended to much lower values of resistance. This may allow a more practical understanding of this phenomena.

Power Production. The peak power generated during an experiment is obtained by squaring the magnitude of the peak of the voltage trace. The peak power is then $P = V^2R$. A graph of peak power for different load resistances is shown in Figure 2.9 for electrodes of different size and position in the channel. It is seen that in the regions where the data overlap the highest power is drawn from the larger electrode. It should be noted, however, that for load resistances less than 0.05 ohms, the power output from the short electrode increases rapidly with lowering load impedance. This is the arc mode region discussed above.

The transition to the arc mode, being dependent upon current density, occurs at a lower load impedance for the long electrode. These data also indicate that the output power for a given impedance level decreases with distance downstream. In the linear conductivity regime the power output is approximately proportional to the electrode area.

Figure 2.10 is a plot of the electrical energy which has been generated per pulse as a function of the load impedance for three different size electrodes. While there is quite a bit of scatter in the data for the 0.50 inch long electrode, the maximum energy for an 0.005 ohm load, scales approximately as the area of the electrode. The maximum energy production has been approximately 2.2 joules. Further work is needed in this area.

The highest values for both power output and energy conversion occurred in an experiment wherein the test channel was

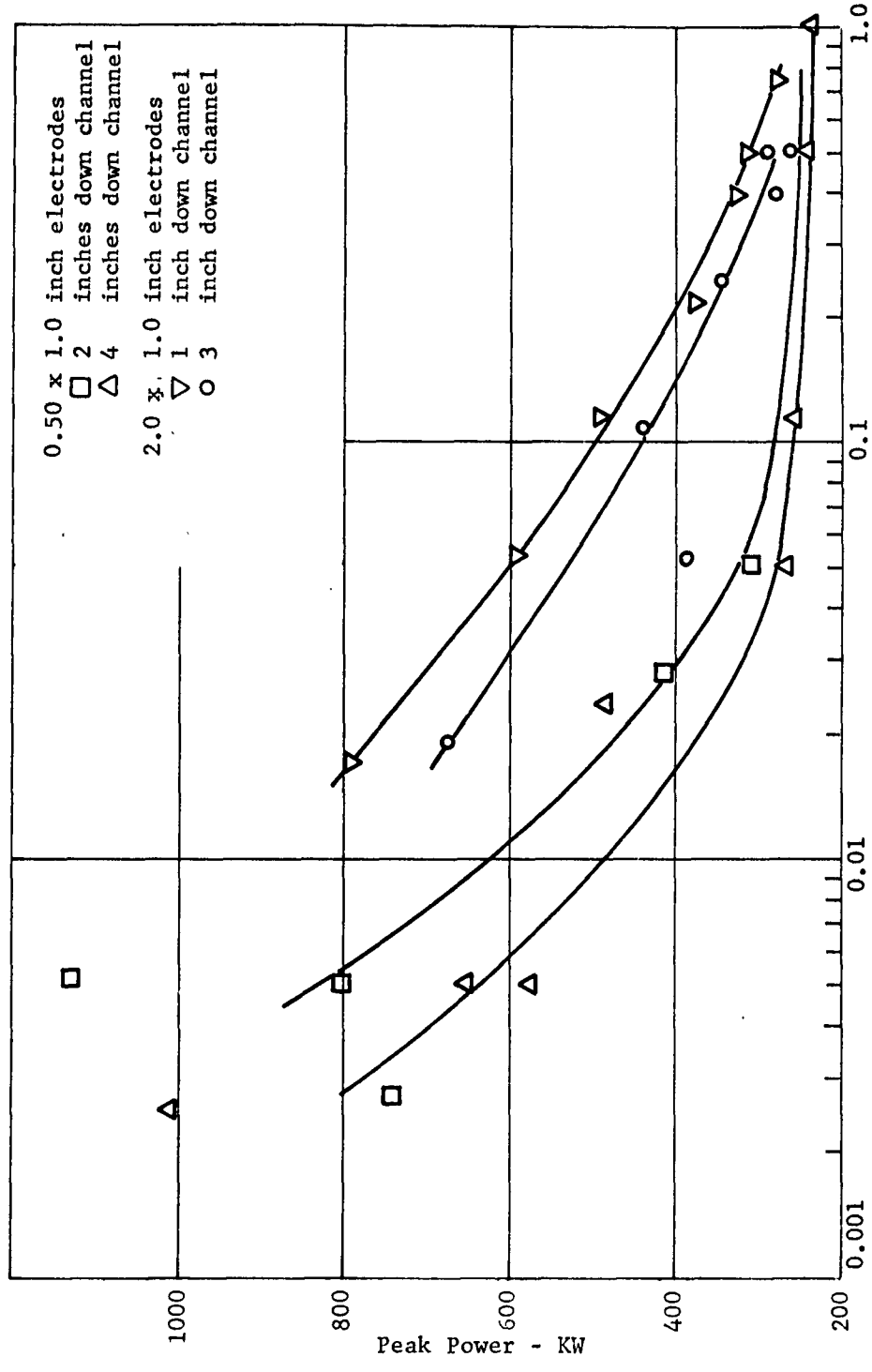

Figure 2.9 Plot showing the peak power as a function of load resistance for electrodes of various sizes and locations along the channel.

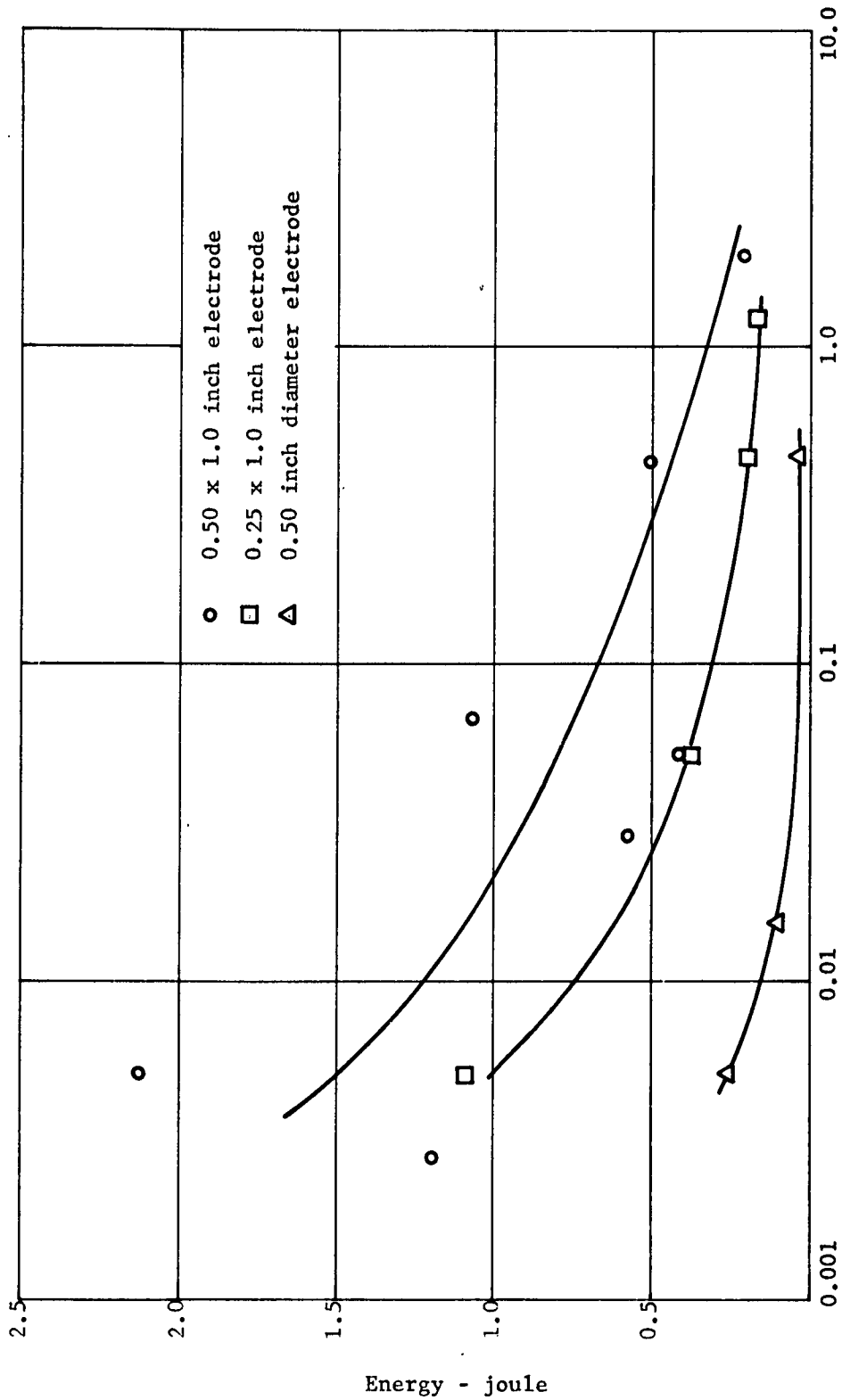

Figure 2.10 Plot of electrical energy output per pulse as a function of load resistance for 3 different size electrodes located 2.0 inches from channel entrance.

evacuated with a vacuum pump to about 1/3 of an atmosphere. The data from this experiment is shown in Figure 2.11, along with data from a comparable series where the channel contained air at atmospheric pressure. It is seen that the peak power production at the first electrode was 1600 KW. The measured peak power decreased with distance down the channel at about the same rate in both cases.

Seeding Method and Concentration. Two methods of seeding the explosive have been investigated. In one method the seed material is externally applied to the surface of the explosive on the inside of the charge cone. In the other method, the seed material is mixed into the bulk explosive and the charges are then pressed into shape. The only seed material which has been thoroughly investigated is cesium picrate, which is an explosive of the non-detonating type.

A comparison of the two methods of seeding indicates that for unconfined RDX charges, the surface seeding method is approximately a factor of ten better than the bulk seeding method in terms of the power output at any particular resistive load. This comparison was made with a ten gram explosive charge of waxed RDX which is equivalent to the duPont 20B perforators.

A preliminary investigation of the power output for various amounts of seed has been performed. For the surface seeding method, amounts between 0.10 gram and 1.0 gram have been used. The power output appears roughly constant between these limits. For the bulk seeding method, amounts between 6% and 24% by weight have been investigated. The power output in this case is also roughly constant for this range of seed level. Type PBX explosive has also been tried with the integrated seeding method. Comparing this explosive with bulk seed to a surface seeded RDX charge indicates the power output of the bulk seeded charge is approximately 70% of the surface seeded charge.

Velocity Measurements. The velocity of the shock waves has been measured by comparing the time of arrival of the shock front at electrode stations in the channel. These time points are compared on dual

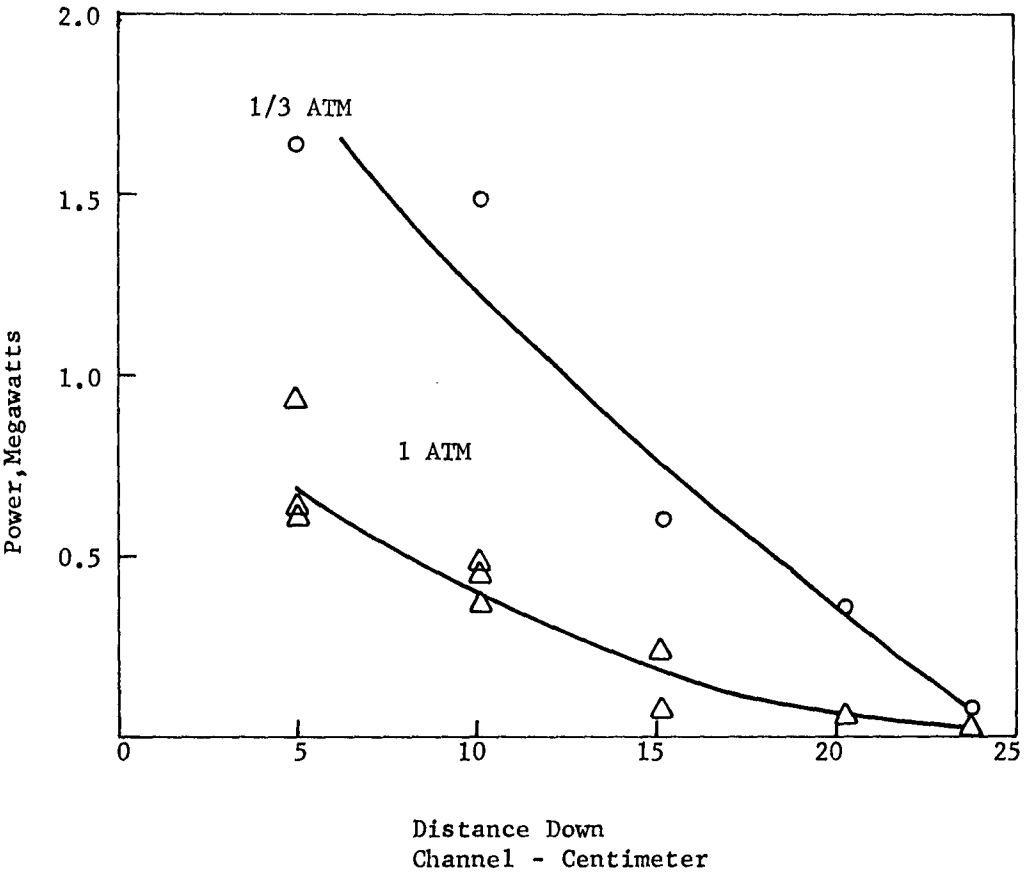

Figure 2.11 Plot of peak power output as a function of distance along the channel showing the effect of a reduction in channel pressure on performance.

beam oscilloscopes that are triggered at the same time. A graph of the elapsed time for the shock to travel down the channel versus the distance down the channel is shown in Figure 2.12. The velocity of the shock front is approximately 6.0 kilometers per second.

The gas velocity behind the shock wave can be determined by measuring the open circuit voltage developed across the electrode for different magnetic field values. The relation for the open circuit voltage is $V_{OC} = UBd$, where U is the gas velocity, B is the magnetic field, and d is the distance between the electrodes. A graph of the measured open circuit voltage (20 megohms load) for various magnetic fields is shown in Figure 2.13. The gas velocity derived from this data is 4.73 kilometers per second.

Results from the experiment wherein the pressure in the test section was 1/3 of an atmosphere of air indicate a slightly higher shock velocity than at atmospheric pressure. The shock velocity obtained by elapsed time from the shock to travel down the channel is shown in Figure 2.14 and indicates a velocity of 6.3 kilometers per second.

2.4 Discussion

From the foregoing it is clear that a fraction of the kinetic energy contained in the detonation products from a seeded, shaped, condensed explosive can be converted into a useful power pulse by MHD techniques. At present, the conversion efficiency is very low, approximately 10^{-4} on the basis of the explosive energy in the charge. However, on the basis of the energy in the explosive jet, the conversion efficiency is of the order of 10^{-2}. It is necessary to use a low ionization potential seed material in order to achieve conversion efficiencies of this order. The power is delivered in a pulse which lasts for approximately 10 microseconds. The maximum power output to date has been 1800 KW.

There are apparently two modes of operation in this type device. For high impedance loads, the device operates as a conventional MHD generator. The specific power output in this mode is about 50 KW/cm^3 in the vicinity of the entrance to the generator, using a

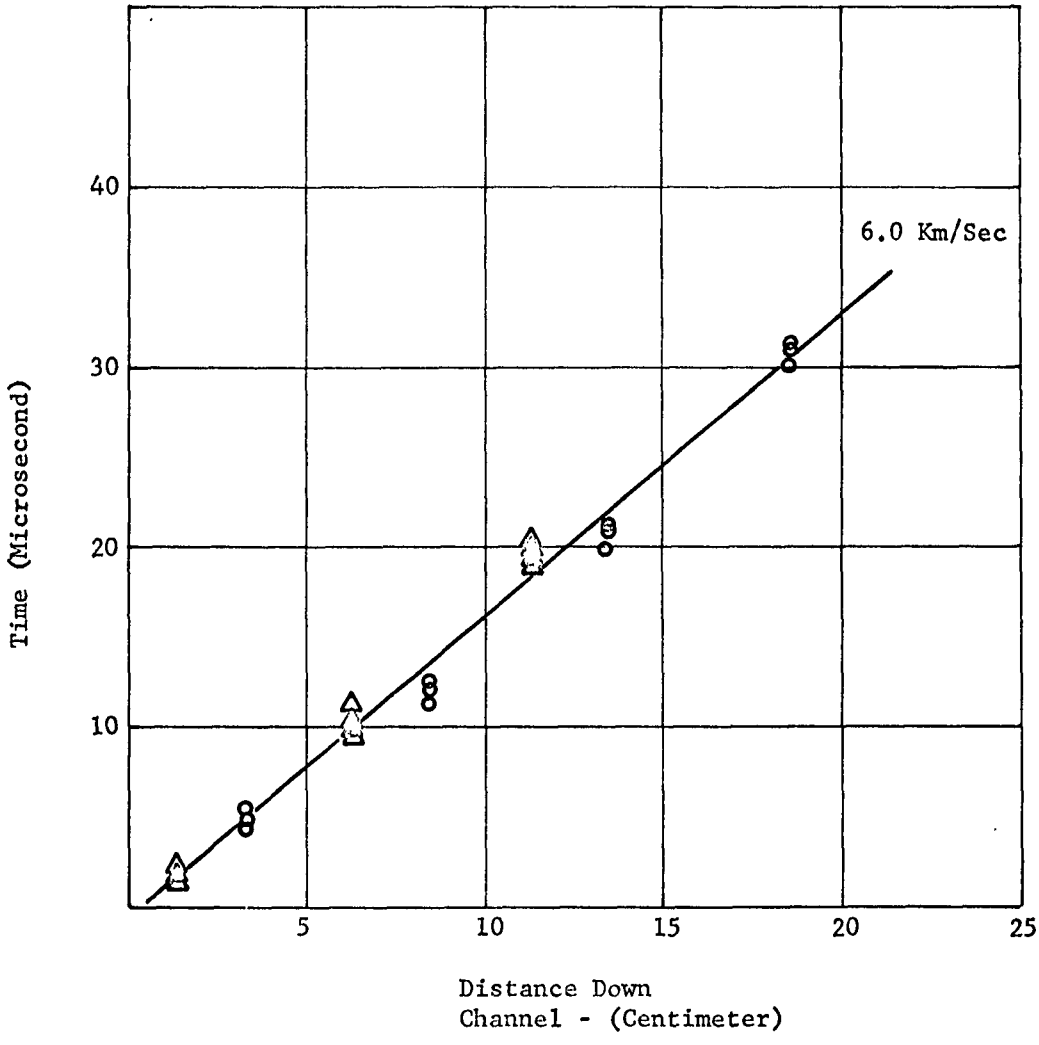

Figure 2.12 Time-distance plot for the explosive-driven shock at atmospheric pressure.

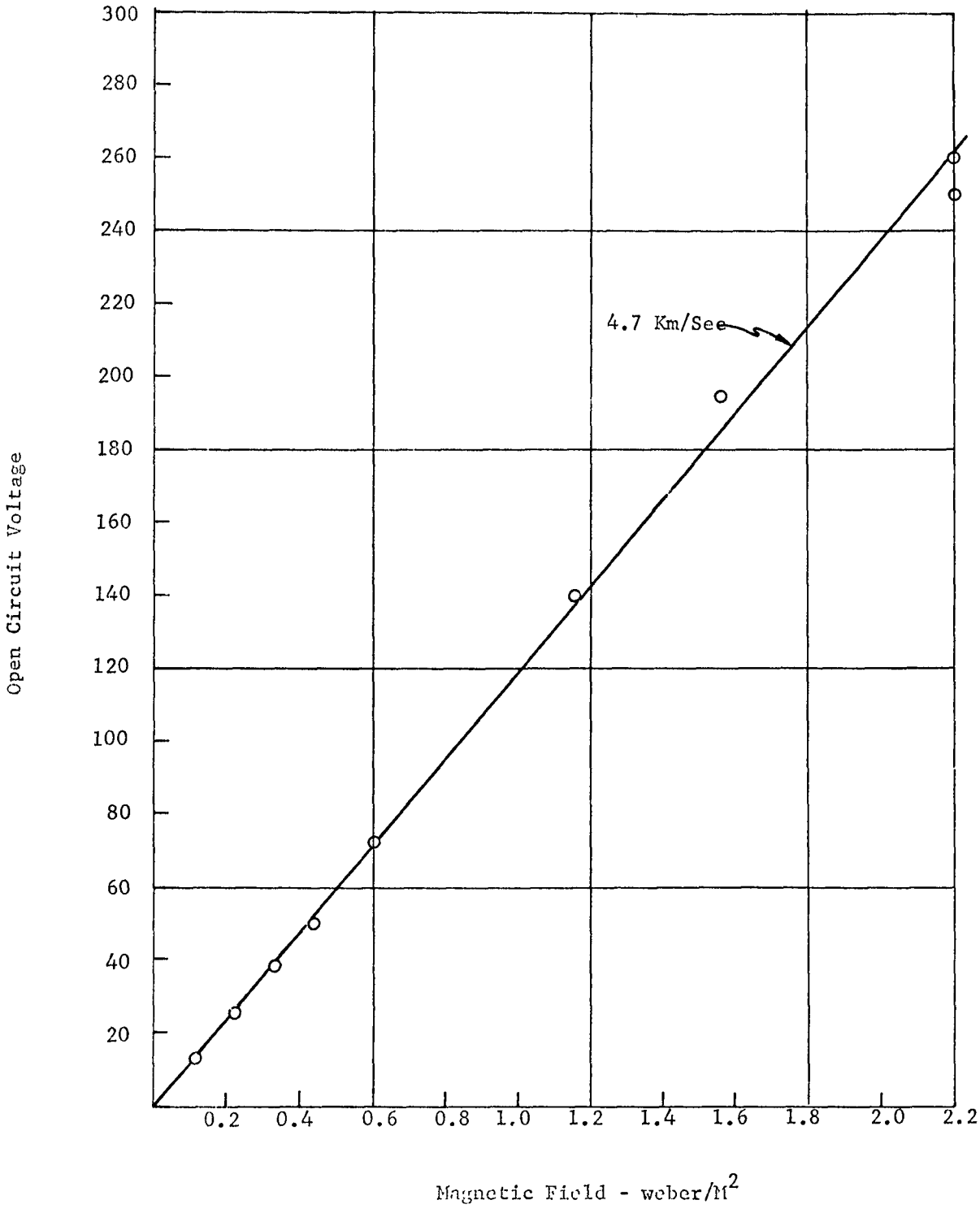

Figure 2.13 Open circuit voltage versus applied field. From this plot the effective gas velocity of 4.7 Km/sec can be determined.

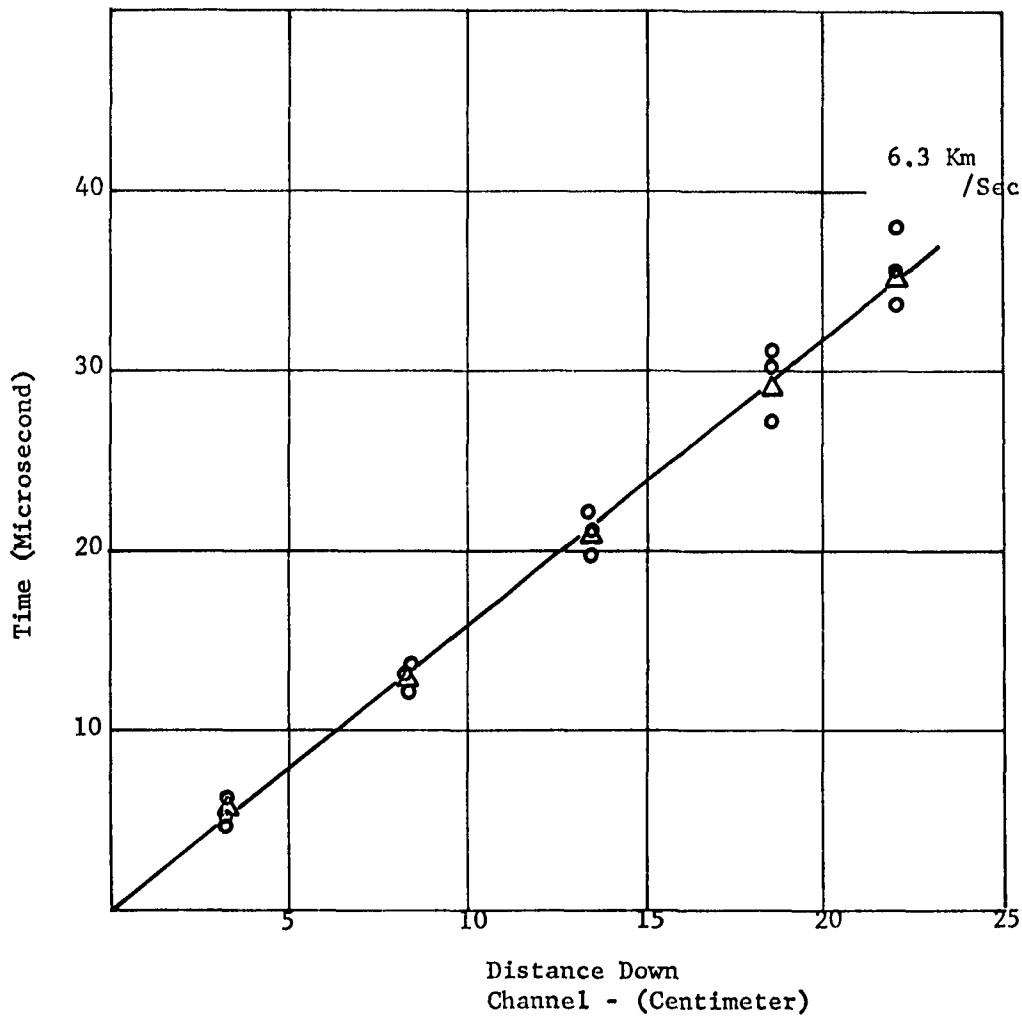

Figure 2.14 Time-distance plot for the explosive-driven shock at a pressure of 1/3 atmosphere.

magnetic field of 22 kilogauss. For low impedance loads, the current-voltage relation becomes non-linear, similar to an electric arc. In the arc mode, the conductivity appears to be an order of magnitude higher than in the linear region. The power output is correspondingly higher.

It is interesting to note that the arc mode generator is extremely attractive for such applications as pulsing a noble gas flash lamp of the conventional type. The starting voltage is a factor of five times the operating voltage across the load which is exactly the desired characteristic for a xenon flash lamp.

A study has been conducted of the problems to be faced in scaling the explosive-driven devices to higher power levels, or in constructing a device in a form other than the conventional linear geometry which has been investigated in the experimental program. The major elements of this study are contained in Appendix A which was prepared by P. Smy and C. N. McKinnon. This study indicates that in scaling the present experiments to a larger size the magnetic Reynolds number, R_m, will approach, or become greater than, unity. When the R_m is greater than unity, the induced (generated) current perturbs the applied field and places an upper limit on the power output of the generator of

$$P_{max} = \frac{2B^2 AU}{\mu_o},$$

where A is the flow cross-sectional area, U is the gas velocity and μ_o is the permeability of the conducting medium. This relation suggests the method to be followed in scaling up the explosive-driven MHD devices. This study indicates that for a generator with dimensions of roughly 1 meter, which uses permanent magnets with a field of 10 kilogauss, power levels of 10^9 watts can be achieved. The total energy production would be of the order of 2×10^5 joules. It is indicated that such devices would be competitive with other pulse power sources.

3. LONG DURATION PULSED POWER

3.1 Introduction

The goal of the experimental program described in this section is to investigate MHD methods of converting stored chemical energy into useful electrical energy in the time range from 1 millisecond to 1 second. The program was initiated in November 1962 as a result of the encouraging results reported in Section 2. The times involved in detonating systems however, are limited to an order of 1 millisecond for any reasonable sized device (5 km/sec x 1 mili sec = 5 meters). It was realized that many applications might require pulse durations up to a few seconds. In order to increase the time scale, slower burning (deflagrating) explosives or solid propellant-type materials are used. In this approach hot gases, seeded with low ionization potential materials, are generated in a combustion chamber, then expanded to achieve a high velocity in the MHD channel. Calculations indicate a conductivity level of the order of 6×10^3 mho/meters in some systems of possible interest.

The program has been divided into several successive phases. The first is to evaluate possible chemical systems for use in this type of generation scheme under actual generation conditions. The second phase is the design of a prototype power generator based upon the best information available from the first phase. A possible third phase would cover the development of a demonstration experiment, complete with generator and power-consuming apparatus. The initial experiments will be restricted to solid ingredients because of the ease of handling and the simplified safety procedures. At some future time after techniques have been worked out, it is planned to use gaseous cyanogen (C_2N_2) and oxygen. The cyanogen flame temperature, $4800^{\circ}K$, is the highest known and should produce the highest conductivities attainable by thermal ionization of low ionization potential materials in chemically reacting systems.

The present experiments are on a laboratory scale with channel dimensions of the order of centimeters in cross-section and 25 centimeters long. At some future date the scale of the experiment will be enlarged if test results indicate that it is necessary to evaluate scaling factors. However, for the use of larger charges, a remote location will be required because of safety considerations.

3.2 Experimental Apparatus

On designing the facilities the approach has been to make the test hardware versatile so that it will be practical to change as many of the gas dynamic parameters as possible. The major objective of the mechanical design has been that the gas should have an extremely high conductivity, by keeping the temperature high, and a high velocity. The important parameter to maximize is the product of the conductivity times the velocity squared. As a first approximation this procedure will result in the maximum power production per unit volume.

The details of the initial facility are shown in Figure 3.1. Figure 3.2 is a photograph of the channel showing the combustion sections, the MHD test section and a flange instrumented for 35 KMC microwave measurements. The hot gas which is seeded with cesium to produce ionization is generated in the combustion section; then expanded through a nozzle to supersonic velocity in the test section region. The test section is designed so that the outer case can be made vacuum tight. The inner parts which form the channel walls are of readily machinable materials such as micarta reinforced plastic laminates, or copper so that the channel geometry can be readily changed to incorporate different flow characteristics. For the initial experiments we have assumed a maximum explosive charge size of 100 grams. In the initial experiments the channel has straight sidewalls so that the channel is of constant width. The channel depth is increased to provide a two-dimensional expansion which is much easier to calculate than for three dimensional geometry.

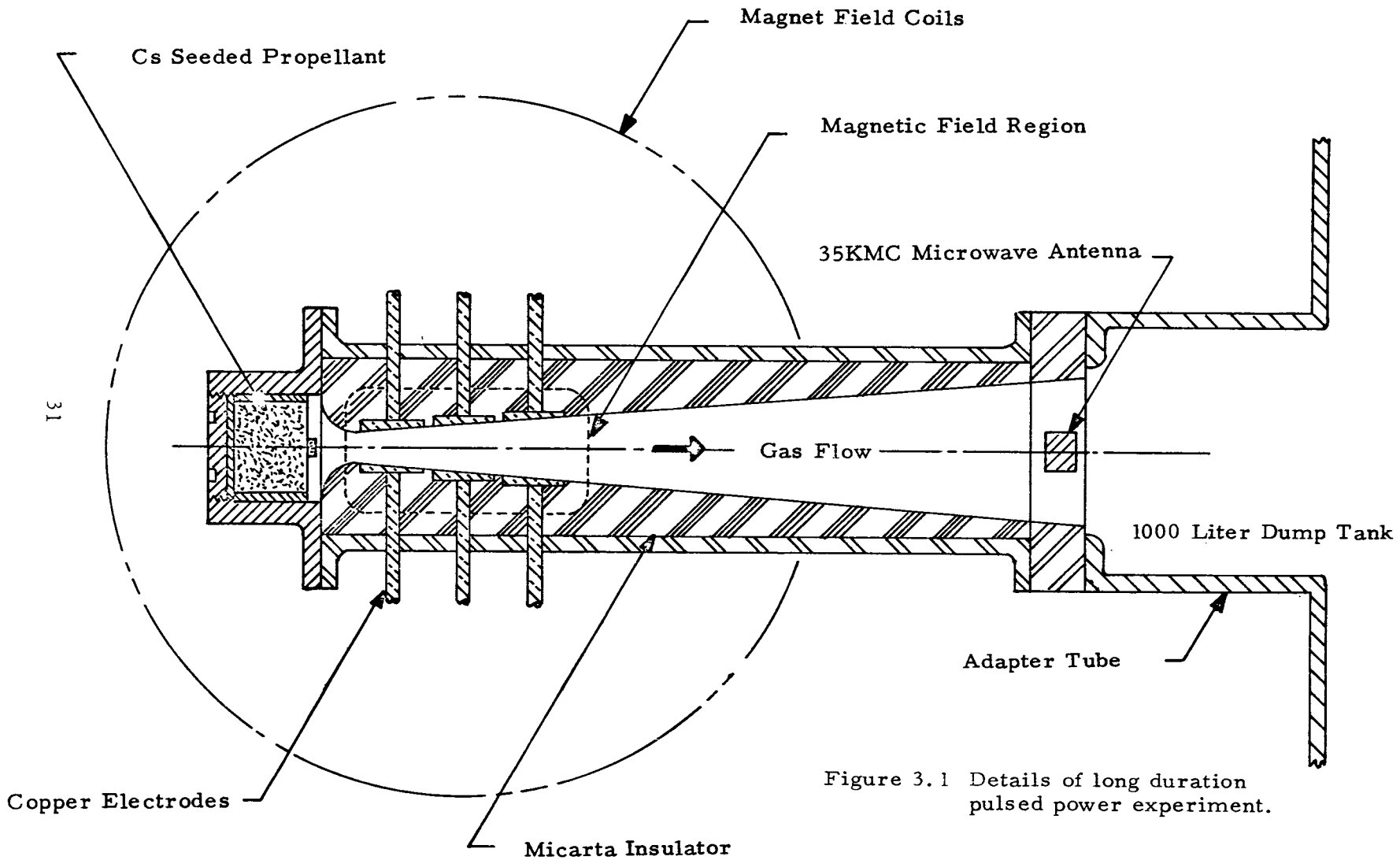

Figure 3.1 Details of long duration pulsed power experiment.

Long Duration Pulse Power Facility

Figure 3.2 Photograph of the hardware for long duration pulsed power experiment.

However, as stated above, three-dimensional expansion can easily be incorporated if deemed necessary. For the channel shown in Figure 3.1, the channel width is 1 inch. The throat area is 0.25 in^2 and the exhaust area is 2.00 in^2. The channel is 10 inches long.

Three pairs of unheated copper electrodes are located in the upstream end of the test section. The Hall effect is expected to be small, because of the low values of magnetic field and high pressures, so that continuous electrodes could have been used. However, the segmented electrodes will allow an assessment to be made of the gas conductivity as a function of distance down the channel. This procedure will be discussed in Section 3.4.

The magnetic field in the initial experiment will be provided by a small electromagnet which can produce fields up to 10 kilogauss, similar to the levels which can be provided by permanent magnets. Another electromagnet, capable of producing 30 kilogauss, is available and can be incorporated into this facility if so desired.

The channel discharges into a dump tank which serves as a receiver for the gaseous products from the flow channel. These gases can be highly corrosive and toxic. The tank is connected to a vacuum pump and can be evacuated, or pressurized, before each shot. Therefore the pressure in the tank serves to regulate the pressure at the downstream end of the channel. The tank contains sufficient volume so that the change in pressure during the burning time of the charge will be of the order of a few per cent.

Provision has been made to install instrument flanges at the downstream end of the channel and in the adapter tube. The microwave flange shown in Figure 3.2 is an example of this instrumentation. Details of the other types of instrumentation will be discussed in Section 3.4.

The first fuel to be used is a standard 75% ammonium perchlorate resin bonded rocket propellant. This is not an optimum choice

for conductivity, but the characteristics of this material have been well documented and the material has been so widely used, that it offers a safe starting point for the experimental program. Some of the pertinent data for this propellant are:

Mol weight	=	22 to 25	
T_F @ 100 psi	=	2600°K	
Density (ρ)	=	1.6 gm/cc = 0.06 lb/ft^3	
Burning rate (r)	=	0.33 in/sec @ 900 psi	(Plateau
	=	0.25 in/sec @ 300 psi	burning
	γ =	1.25	type)

Two varieties of the propellant are to be tried. In addition to Cs seed, some charges will have about 10% by weight aluminum powder added. In addition to raising the flame temperature, the aluminum buffers the reaction so that the burning continues for some period of time as the gas flows down the channel. The net effect is that the gas temperature in the channel is somewhat higher than would have been expected on the basis of expansion of the gases at the burning temperature.

By placing fine wires in the cast propellant, the burning surface area can be increased to give an equivalent rate, r, of about 1 in/sec or greater at the pressures of interest, say 1000 psi. Assuming an end burning grain with a surface area, S, of 11.5 cm^2 (1-1/2 in dia), and burning at 1000 psi, the mass flow rate is,

$$\dot{m} = \rho S r = 1.65 \frac{gm}{cm^3} \times 11.5\ cm^2 \times 2.54\ \frac{cm}{sec} = 50\ gm/sec\ .$$

The requirement for stable burning is constant chamber pressure. The sonic throat area that will maintain 1000 psi at this flow rate is approximately

$$A = \frac{\dot{m}\sqrt{g\,\gamma\,RT}}{pg\gamma\sqrt{\left(\frac{2}{\gamma+1}\right)^{\frac{\gamma+1}{\gamma-1}}}} = .15 \text{ in.}^2$$

for

$P = 1000$ psi

$\dot{m} = 50$ gm/sec $= 0.11$ lb sec.

$T = 4600^{\circ}R$

$\gamma = 1.25$

$g = 32$ ft/sec^2

$R = 1544$ ft-lb/$^{\circ}$R mole

$M = 25$ lb/mole

This means that the nozzle throat has to be 0.150 in. x 1.00 in. This is extremely small compared to the other dimensions of the channel. It is therefore planned to increase the throat area to 0.250 in^2 which should produce a chamber pressure around 500 psi. It should be noted that the ammonium perchlorate propellant still maintains a high burning rate at this pressure because of the plateau-type characteristic. The wires in the propellant as described above should also help control the chamber pressure. Blowout plugs in the combustor will prevent damage if any combustion oscillation or tendency to detonate occurs. Ignition of the propellant is accomplished by electric ignitor squibs on the face of the grain. For burning a time duration of about 1 sec, the grain will have to be about 1 inch long which is the approximate dimension of the combustion chamber.

For the first experiments the propellant is seeded with about 1% $CsCO_3$. At the entrance to the test section calculations indicate that the conductivity should exceed 50 mho/meter. The pressure at the entrance to the test section should be of the order of 150 psi or below, since the throat pressure is approximately 0.55 of the stagnation pressure, which is about 500 psi. The Mach number at the exit will be the value for

approximate isentropic flow which in this case is 3.3 (for $\gamma = 1.25$). The chlorine present from the perchlorate should have a strong negative effect on the conductivity because of electron attachment to form Cl_2^- ions as the temperature is decreased below the flame temperature of 2600°K. The exit pressure will be approximately equal to one eighth of the stagnation pressure which implies an exit temperature in the neighborhood of 1200°K. Therefore, the exit gas should have a vanishingly small conductivity.

It is expected that the specific power output of the test facility when using cesium seeded ammonium perchlorate with a magnetic field of 10 kilogauss, will be of the order 25 watts/cm^3. If the volume of the working section of the generator is assumed to be 41 cm^3 (the magnetic field region volume), the predicted output power using ammonium perchlorate is about 1 KW. If the power is produced for 1 second, the net output will be about 1 kilojoule. Considering the energy stored in the fuel, at roughly 1 kilocalorie per gram, or 200 kilojoules for 50 grams, the expected conversion efficiency is of the order of 1%. It should be noted that the ammonium perchlorate propellant is being used primarily to test out the facility and instrumentation, and does not represent the maximum power generating capability. Propellant mixtures more suitable for the stated purposes will be discussed in Section 3.3.3.

3.3 Consideration of Possible Chemical Systems

For comparison purposes, the power output of a given MHD channel using a certain type of propellant material will be an index of the suitability of this material for the purposes stated. Other considerations such as storability, toxicity, etc., may play a role in the final selection of the system to be used. Therefore the ability of a certain propellant to generate high power level per unit volume of channel is a necessary, but not necessarily sufficient, condition for its selection for use.

Inasmuch as the time duration of these experiments are short in terms of thermal time constants, heat transfer and attendant material problems are not a major concern. The burning chemical system then can be chosen to maximize the conductivity in the channel region. This means that temperature in the moving gas should be maximized. To a first approximation the conductivity is dependent upon the charge carrier density which is described by the Saha equation as a function of electron temperature and ionization potential of seed material.

The following paragraphs describe some of the criteria which have been used in choosing chemical systems which should result in a channel working fluid with maximum conductivity.

3.3.1 Systems with a low molecular weight gas product are desired so that a high gas velocity can be obtained with a minimum of temperature drop in the channel. The reason for the high velocity requirement is that the power output per unit volume of channel varies as the gas velocity squared. It is expected that diatomic detonation products such as CO, O_2, NO, and N_2 with a mean molecular weight in the range between 25 and 30, will have a reasonably high sound speed, compared to hydrocarbon combustion products where CO_2, with molecular weight of 44, is a major component. Sound velocity varies inversely as the square root of the molecular weight. With high sound speed, the gas velocity will be higher for a given Mach number.

3.3.2 The second desirable quality is a low momentum transfer cross-section for the gas products. Diatomic molecules are much preferred over triatomic molecules such as CO_2 or H_2O which result from complete combustion of hydrocarbons.

3.3.3 To maximize the gas temperature in the channel, products with high dissociation potentials are desirable. N_2 and CO are desirable in this respect.

3.3.4 Since the currents in MHD devices are generally carried by the electrons, any electronegative, or electron attaching gases should be avoided. Since most electronegative species have an attachment potential below 3.5 ev, electron attachment should not be a major problem if the gas temperature is above 3500°K.

3.3.5 A system that produces solid carbon or some other contaminate is undesirable inasmuch as the solid materials may reduce electrode efficiency or short-out insulators. Two phase systems such as the aluminum-cesium nitrate system which has as a reaction product liquid Al_2O_3 may pose a practical problem even though the calculated electron yields of such systems are reported to be very high.[3]

3.3.6 The burning rate of the system should be variable to get event times from 1 mil sec to 1 sec. Grain size variation is a common method. In no case should the system detonate.

3.3.7 The free electrons should be produced by the thermal ionization of Cs or other low ionization potential metal such as potassium added to the chemical system in the form of either exothermic or endothermic salts; $CsCO_3$ and CsN_3 are endothermic, while Cs picrate, $CsNO_3$, and CsO_3 are exothermic. $CsCO_3$ is the least expensive of the cesium salts. It should be noted that some systems (see Table I) have built-in seed.

The highest known flame temperature is that due to C_2N_2. The adiabatic flame temperature is 4850°K at 1 atmosphere. Seeding this flame with Cs to 1% molar levels should result in 10^{16} electrons/cm^3. Since the reaction products are the diatomic molecules CO and N_2, the mobility is on the order of 3 m^2/volt-sec. Neglecting Coulomb scattering the conductivity should be then

$$\sigma = n_{eq}\mu = 10^{16} \times 1.6 \times 10^{-19} \times 3 \times 10^4 =$$

$$= 4800 \text{ mho/meter}.$$

Cyanogen is liquid or gas at room temperature, depending upon the pressure, and is extremely poisonous. Because of the hazard involved, cyanogen experiments will only be conducted after a full evaluation of the hazards, and a clear indication from the experimental program that the high temperatures of the cyanogen flame are required.

A promising solid system which meets the criteria discussed above is:[3]

$$3C_2N_6O_{12} + 5C_6N_4 + 3CsN_3$$

(hexanitroethane) + (tetracyanoethelene) + (cesium azide)

$$\longrightarrow 36CO + 23.5\,N_2 + 3\,Cs$$

This system produces gases with average molecular weight of 33 at 3500°K and 1 atmospheric pressure. About 10% of the cesium ionizes by the reaction $Cs \rightleftharpoons Cs^+ + e^-$ to produce 1/2 mole %, or 10^{16} electrons/cm^3. The conductivity should be in the range of 1500 to 3000 mho/meter, which is slightly lower than in the seeded cyanogen flame.

Another promising system which is used by Atlantic Research[3] for the generation of electrons is the reaction

$$2\,Al + Cs\,NO_3 \longrightarrow Cs + Al_2O_3 + \tfrac{1}{2}\,N_2$$

Friedman has calculated that this system produces 2.4% electrons (based on gas) while burning at 3700°K and 1 atmosphere. There are several possible drawbacks to this system. It is expected that the large total cross-section of increased number of cesium atoms , and the cross-section of the complex Al_2O_3 molecule, should result in a much lower conductivity than that obtained for a comparable electron density in the cyanogen systems. The Al_2O_3 also liquifies at 3700°K acting as a contaminate. The liquified Al_2O_3 will have approximately 35% of the gas momentum in a non-transferable phase which makes the calculation of channel flow characteristics

somewhat complicated. The full implications of the Al_2O_3 on all parts of the system (nozzles, electrodes, insulators, flow characteristics, etc.), have not been evaluated.

Table 1 summarizes some of the systems which have been considered. The main emphasis in the experimental program is on obtaining a suitable solid system which is easy to handle and which yields contaminate-free products of the highest conductivity.

TABLE 1

VARIOUS PROPELLANT SYSTEMS YIELDING CONDUCTIVE GASES

Trade Name	Basic Ingredients / Main Proudcts	Seed	Product Phase	Flame Temp °K @ Pressure	Estimated Ne/cm^3	Expected Conductivity (mho/meter)	References
AK (75% Ammonium Perchlorate)	$NH_4ClO_4 + C_2H_4O$ / $HCL + CO_2 + H_2O$	Cs	Gas	2600 @ 500 psi	10^{14}	50	(7)
JPN (Ballistite)	$C_6H_7O_2(ONO_2)_3 + C_3H_5(ONO)_3$ / $CO_2 + H_2O + N_2$	Cs	Gas	3100 @ 500 psi	10^{15}	200	(7)
Acetelene, oxygen (gas)	$C_2H_2 + O_2$ / $H_2O + CO_2$	2 mol % K	Detonation in gas	3600 4 atm	--	270 (measured)	(6)
Cesium nitrate, aluminum	$CsNO_3 + Al$ / $Al_2O_3 + Cs + N_2$	--	.65 gas .35 liq	4162 @ 8 atm	2.7×10^{17} *	10^3	(3)
Cesium nitrate, yttrium	$CsNO_3 + Y$ / $Y_2O_3 + Cs + N_2$	--	.65 gas .35 liq	4870 @ 8 atm	5.8×10^{17} *	10^3	(3)
Tetracyano-ethylene hexanitro-ethane	$C_2N_6O_{12} + C_6N_4$ / $CO + N_2$	CsN_3 to 10%	Gas	3500 @ 1 atm	10^{16}	ca 5×10^3	(3)
Cyanogen, oxygen (gas)	$C_2N_2 + O_2$ / $CO + N_2$	0-10% Cs	Gas	4850 @ 1 atm	$10^{15} - 10^{17}$	10^4	(4) (5)

*Based on gaseous phase

3.4 Instrumentation

3.4.1 Measurement of Conductivity. In the previous section we have reviewed several of the possible chemical systems. From the predicted electron densities and mobilities it can be seen that the conductivity σ is variable over a wide range, and is difficult to calculate. Conductivity is the most important gas parameter in the power generation process. Since it is such a strong function of temperature, it is felt that the conductivity should be determined for each system as accurately as possible.

It is intended to measure conductivity primarily from the slope of the characteristic voltage versus current (V-I) curves. It is realized that the true conductivity will be masked by generator end effects, sheath voltage drops, Hall effects, and fringing effects. However, auxiliary experiments can be used to evaluate the correction factors needed to obtain the true conductivity from the V-I curves. The largest corrections are expected to be because of an electrode sheath drop at the cold copper electrodes. Since the generated potentials will be on the order of 10 V/cm across 2 - 3 cm, open circuit voltages of no more than 40 volts are expected with 10 kilogauss magnetic fields. Electrode drops for the several ampere currents expected could be a large fraction of this value. One way to evaluate this effect is to apply external potentials which greatly exceed the expected sheath drop. These potentials can be derived from batteries. If batteries are used, only one data point per electrode pair per shot will result. An alternative procedure is to use low frequency (60 cycles) alternating current potentials. For a shot duration of one second, at least 10 or so cycles will represent steady-state conditions and each cycle is a complete V-I curve from which electrode drop and plasma resistance can be determined.

3.4.2. Microwaves. In support of the foregoing conductivity measurements, a 35 KMC microwave system is available for use on the flow channel. It is to be used for attenuation measurements at

the downstream end of the diverging channel where the gas density will always be at a minimum (assuming supersonic flow). Figure 3.3 is a plot of microwave attenuation versus electron density for 9 KMC and 35 KMC signals, for an assumed collision frequency of 2×10^{11} sec^{-1}. For an electron density of $10^{13}/cm^3$, an attenuation of 1.5 nepers per cm is predicted.

3.4.3 Gas Temperature Measurements. In the first phase of the program the gas temperature will not be measured. The conductivity is of primary interest, and the system can be evaluated on that factor alone. Temperature can be estimated from thermodynamic data on each system. Alkali metal resonant line reversal temperature measurement systems are available for use if required for a complete understanding of any chemical system.

3.4.4 Pressure Measurements. In the combustion chamber area, the pressure will be measured by 0-3000 psi fast response strain gage transducer. This measurement is mainly to determine the combustion rate and the mass flow rate. A similar transducer is also mounted at the exit of the test section to determine the pressure drop so that the velocity can be calculated.

3.4.5 Recording System. The data from the various sensors and the voltages across the load resistors and current shunts will be recorded on a Consolidated Electrodynamics Corporation Model 5-114 Multichannel Recorder. Up to 18 channels can be recorded simultaneously. Fluid damped galvanometers capable of 100 cycles per second response are available.

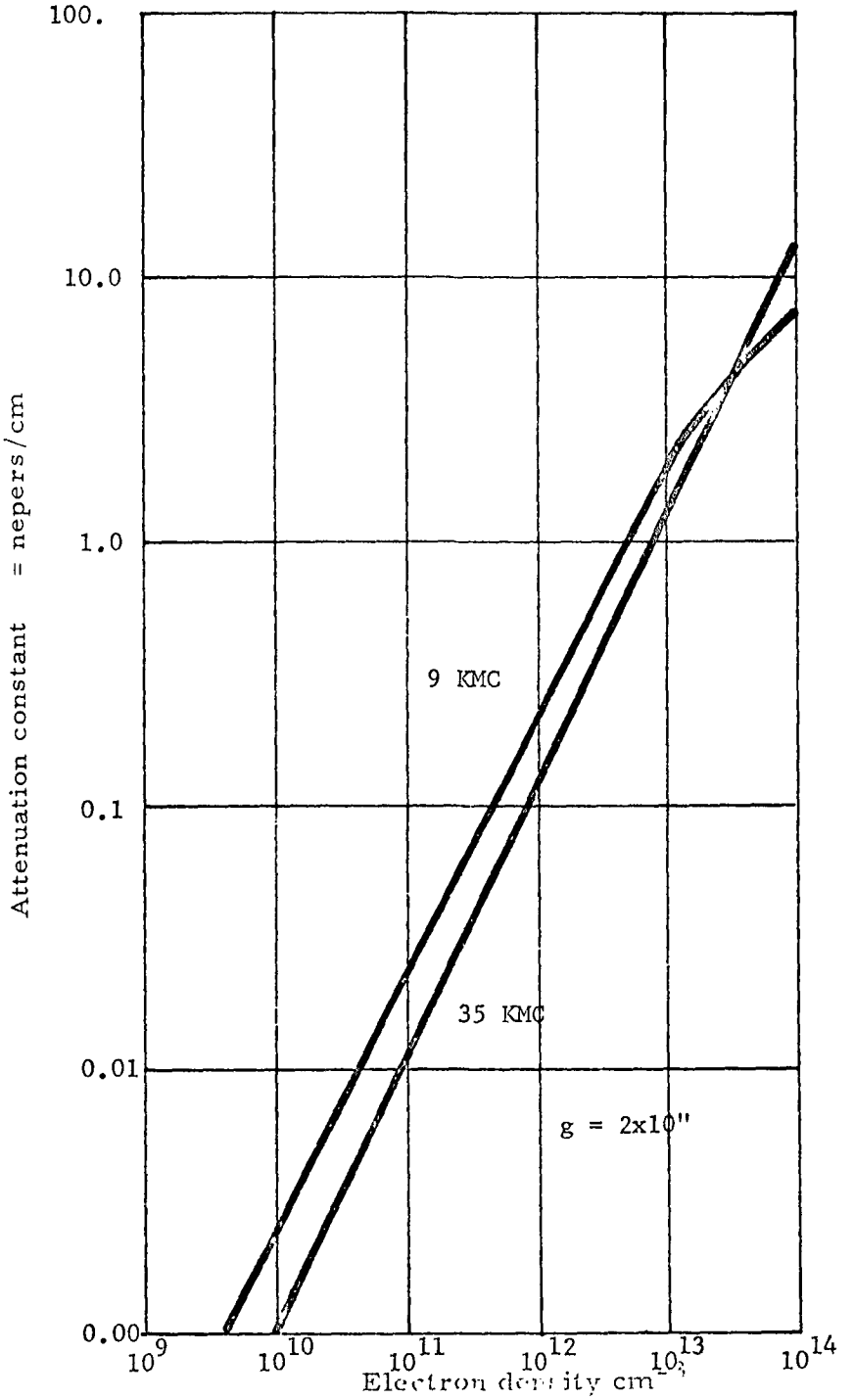

Figure 3.3 Plot of microwave attenuation versus electron density for 9 KMC and 35 KMC test frequencies. A collision frequency of 2×10^{11} A sec^{-1} has been assumed.

4. COMBUSTION PRODUCT STUDIES

4.1 Introduction

At the conclusion of Contract Nonr 3523(00), a number of topics were left in a state of partial completion. Machine calculations had indicated the possibility that electron affinity in an electronegative gas combined with buffering reactions might lead to almost complete electron attachment, with a corresponding change in gas conductivity. For typical conditions in a seeded combustion product flow, with seed level on the order of 1%, the calculations indicated that it would be difficult to tell the difference between conduction due to electronic conductivity, with 1% of the seed material ionized, and ionic conductivity with approximately all of the seed material ionized to form positive and negative ions. In the latter case, the two orders of magnitude increase in charge carrier density would just about compensate for the lower mobility of the ions.

In order to investigate this possibility, two different approaches were followed. The first procedure was to manually repeat the machine calculations using the assumed value of 2.1 ev for the electronic attachment energy to form OH^- ions, for one initial input condition with gas temperatures of 2400° and $2800^{\circ}K$. This calculation is discussed in detail in Section 4.2. The second approach was to measure the conductivity of combustion products at two different microwave frequencies, so that the collision frequency for momentum transfer could be determined. Since the electron and ion collision frequencies differ by a factor of about 10^2, this type of measurement, if the test frequency is greater than the collision frequency, allows the assessement of the identity of the principle charge carrier. These measurements are discussed in Section 4.3. This phase of the program is considered as completed and no further work is planned.

4.2 Electron Attachment Studies

Hand calculations of the equilibrium chemical composition of the hydrogen-oxygen flame at two temperatures, 2400 and 2800°C, were carried out to check the validity of the machine calculations which were discussed in the final report on Contract Nonr 3539(00).

The approach used was to calculate the equilibrium constants of each of the reactions from the partition function of each of the reactants. This method was adopted in preference to the use of the Saha approximation, which is generally accurate for an ionization reaction, but leads to a considerable error when the reaction is one of dissociation of a diatomic or polyatomic molecule.

The mechanics of the solution are as follows: consider a general reversible equilibrium reaction (A) plus (B) combining to form (AB), and (AB) dissociating to form (A) and (B) - this reaction proceeding with an energy D, in an isolated, insulated volume V:

$$A + B \underset{}{\overset{D}{\rightleftharpoons}} AB.$$

The equilibrium reaction constant K describes the population of each specie by the following relationship:

$$K = \frac{Z_A Z_B}{Z_{AB}} \exp(-D/kT) = \frac{N_A N_B}{N_{AB}}$$

where

Z's	=	total partition functions of species A, B, & AB
D	=	reaction energy
k	=	Boltzmann's constant
T	=	equilibrium temperature
N_X	=	total number of specie X.

The total partition function of any specie is the product of the translational, electronic, retational, vibrational, and nuclear partition functions. In most reactions the nuclear partition function is omitted, since the nucleus is unchanged in low energy reactions. Saha's approximation considers only the translation partition function.

The individual partition functions are described by:

Translational Partition Function (Z_t)

$$Z_t = \Theta \frac{V}{h^3} (2\pi m_s kT)^{3/2} ,$$

where

Θ = A constant; Θ = 1 for atoms and molecules,
Θ = 2 for electrons.

V = total volume of domain of reaction,

h = Planck's constant,

m_s = mass of specie under consideration.

Note: Z_t is generally divided by the total volume of the reaction domain, yielding ultimately reactant density per unit volume.

Electronic Partition Function (Z_e)

$$Z_e = \sum_{n=o}^{\infty} g_n \exp(-En/kT),$$

where

g_n = statistical weight of the n^{th} spectral term (energy level).
g_o, statistical weight of the ground state.

E_n = energy of the n^{th} spectral term.

Note: If no spectral terms having energies low compared to the equilibrium temperature being considered exist, then only g_o is used, with this

restriction

$$Z_e \simeq g_o .$$

Rotational Partition Function (Z_r)

$$Z_r = \frac{1}{\sigma} \sum_{j=0}^{\infty} (2J+1) \exp(-J(J+1)\hbar^2/2IkT),$$

which can be approximated as

$$Z_r \simeq \frac{1}{\sigma}\left[\frac{T}{T_r} + \frac{1}{3} + \frac{1}{15}\left(\frac{T_r}{T}\right) + \frac{4}{315}\left(\frac{T_r}{T}\right)^2 + \frac{1}{315}\left(\frac{T_r}{T}\right)^3 + \cdots\right],$$

where:

σ = A diatomic molecular constant dependent upon the nature of the molecule

σ = 1 for A $\neq$ B (e.g., OH, HCl, etc.)

σ = 2 for A = B (e.g., O_2, H_2, etc.)

J = Total angular momentum of the atom,

$\hbar = \frac{h}{2\pi}$,

I = moment of inertia of the specie,

$T_r = \frac{\hbar^2}{2Ik} \doteq \frac{Bhc}{k}$, rotational temperature,

$B = \frac{\hbar}{8\pi^2 cI} = \frac{2.7994 \times 10^{-3}}{I}$, (B's most often tabulated),

c = velocity of light in vacua.

Note: If $T \gg T_r$, then $Z_r \simeq \frac{1}{\sigma} \cdot \frac{T}{T_r} \simeq \frac{0.6951}{\sigma} \cdot \frac{T}{B}$;

otherwise $T_r = \frac{\hbar^2}{2Ik} = \frac{Bhc}{k} = 1.439\ B.$

Vibrational Partition Function (Z_v)

$$Z_v = \left[1 - \exp(-h\nu/kT)\right]^{-1} \quad , \text{ or } \quad Z_v = \left[1 - \exp(-T_v/T)\right]^{-1} \quad .$$

where

ν = vibrational frequency

$T_v \equiv \frac{h\nu}{k} = \frac{hc\omega_i}{k}$; (ω_i is most often tabulated),

$T_v = 1.439\omega_i$.

The equilibrium constant, K , can be expressed in several ways; the partial pressure (in atmospheres) notation was selected. The K described above yields a ratio of the number of reactants per unit volume; since CGS units were used throughout, this is number per cm^3. To transform this to a pressure, multiply by kT to obtain, in CGS units, dynes per cm^2. The conversion to atmospheres is 1 atmosphere $= 1.0132 \times 10^6$ dynes/cm^2. Then

$$K_{p_a} = \frac{kT}{1.0132 \times 10^6} \frac{Z_A Z_B}{Z_{AB}} \exp(-D/kT).$$

The most likely reactions occurring in a seeded hydrogen-oxygen flame are:

1. $AOH \rightleftharpoons A + OH$ (A = any alkali), $K_1 = \frac{p(A)\, p(OH)}{p(AOH)}$;

2. $A \rightleftharpoons A^+ + e^-$, $K_2 = \frac{p(A^+)\, p(e^-)}{p(A)}$;

3. $HOH \rightleftharpoons H_2 + \frac{1}{2} O_2$, $K_3 = \frac{p(H_2)\, p(O_2)^{1/2}}{p(HOH)}$;

4. $HOH \rightleftharpoons \frac{1}{2} H_2 + OH$, $K_4 = \frac{p(H_2)^{1/2}\, p(OH)}{p(HOH)}$

5. $OH \rightleftharpoons O + H$, $K_5 = \frac{p(O)\, p(H)}{p(OH)}$;

6. $OH^- \rightleftharpoons OH + e^-$, $\quad K_6 = \dfrac{p(OH)\,p(e^-)}{p(OH^-)}$;

7. $H_2 \rightleftharpoons H + H$, $\quad K_7 = \dfrac{p(H)^2}{p(H_2)}$;

8. $O_2 \rightleftharpoons O = O$, $\quad K_8 = \dfrac{p(O)^2}{p(O_2)}$.

Much of the data required to calculate the reaction constants is unfortunately unavailable for alkalis, hydroxides, hydroxyls, and water. So for the two modes of dissociation of water, values of K(T) were taken from "Combustion, Flames, and Explosions of Gases" by B. Lewis and G. Von Elbe. The K's for the alkali hydroxides were calculated using the approximation of L. S. Frost's "Conductivity of Seeded Atmospheric Pressure Plasmas".(8) The total partition function of OH^- was calculated to agree with the partition functions of O & H from K_7 and K_8.

Since the input conditions were defined as 1% seed (by weight) at one atmosphere, four more equations are provided:

9. $\dfrac{N(H)}{N(O)} = C_1$ (Hydrogen to oxygen ratio is constant.) ,

10. $\dfrac{N(H)}{N(A)} = C_2$ (Hydrogen to alkali ratio is constant.),

where

$$N(H) = c\left[2p(HOH) + p(AOH) + 2p(H_2) + p(OH) + p(OH^-) + p(H)\right] ,$$

$$N(O) = c\left[p(HOH) + p(AOH) + 2\,p(O_2) + p(OH) + p(OH^-) + p(O)\right] ,$$

$$N(A) = c\left[p(AOH) + p(A) + p(A^+)\right] .$$

Specie	Partial Pressure at T = 2400°K	2800°K
HOH	9.350×10^{-1}	7.790×10^{-1}
OH	1.380×10^{-2}	5.460×10^{-2}
H_2	3.201×10^{-2}	9.300×10^{-2}
H	2.842×10^{-3}	2.491×10^{-2}
O_2	1.184×10^{-2}	3.713×10^{-2}
O	1.010×10^{-3}	1.116×10^{-2}
OH^-	3.231×10^{-6}	1.554×10^{-5}
KOH	2.741×10^{-3}	1.204×10^{-3}
K	1.559×10^{-3}	2.702×10^{-3}
K^+	1.663×10^{-5}	1.175×10^{-4}
e^-	1.340×10^{-5}	1.020×10^{-4}
Error in total pressure	+ 0.08%	+ 0.4%
Error in H:O ratio	+ 0.3	-0.6

Table 4.1

Partial Pressure of Species Present in Hydrogen-Oxygen Flame at Temperatures of 2400° - 2800°K

11. $p = p(HOH) + p(AOH) + p(H_2) + p(O_2) + p(OH) + p(OH^-) + p(H) + p(O)$

$+ p(A) + p(A^+) + p(e^-) = 1$ atmosphere.

12. $p(A^+) = p(OH^-) + p(e^-)$, (charge conservation, assuming single ionization.)

These relationships yield 12 equations in 11 unknowns, an over-specification which allows one equation to be used as a check; in this case equations 9 and 11 were used.

The method of solution is outlined in the following flow chart; it is essentially one of trial and error, (see figure 4.1).

The quantities enclosed in circles are trial assumptions. The notation "Restricted Assumption" means that a value of p(HOH) will determine a range of p(OH), through K_4; if this range is exceeded fictitious values of $p(H_2)$ result from K_4 equation.

In this solution the electron attachment energy of OH was assumed to be 2.1 ev, in agreement with the paper by Frost, and consistent with what were believed to be the input conditions to the machine calculations mentioned previously. Table 4.1 gives the partial pressures of the various species present in the hydrogen-oxygen flame at the temperatures of 2400 - 2800°K. The data in this table can be compared with the data presented in Figure III-1 of Reference 1.

As an exercise, to show the sensitivity of OH attachment to attachment energy, as this energy is presently rather poorly defined, four curves of K as f(D) are presented in Figure 4.2. These curves indicate the trend of any reaction, but they specifically describe $OH^- \rightleftharpoons OH + e^-$.

Comparison of the tabulated results from this calculation with the results of the machine calculation presented as graphs in Reference 1 indicates that although the partial pressures for most of the chemical constituents are in good agreement, the effects of electron attachment were

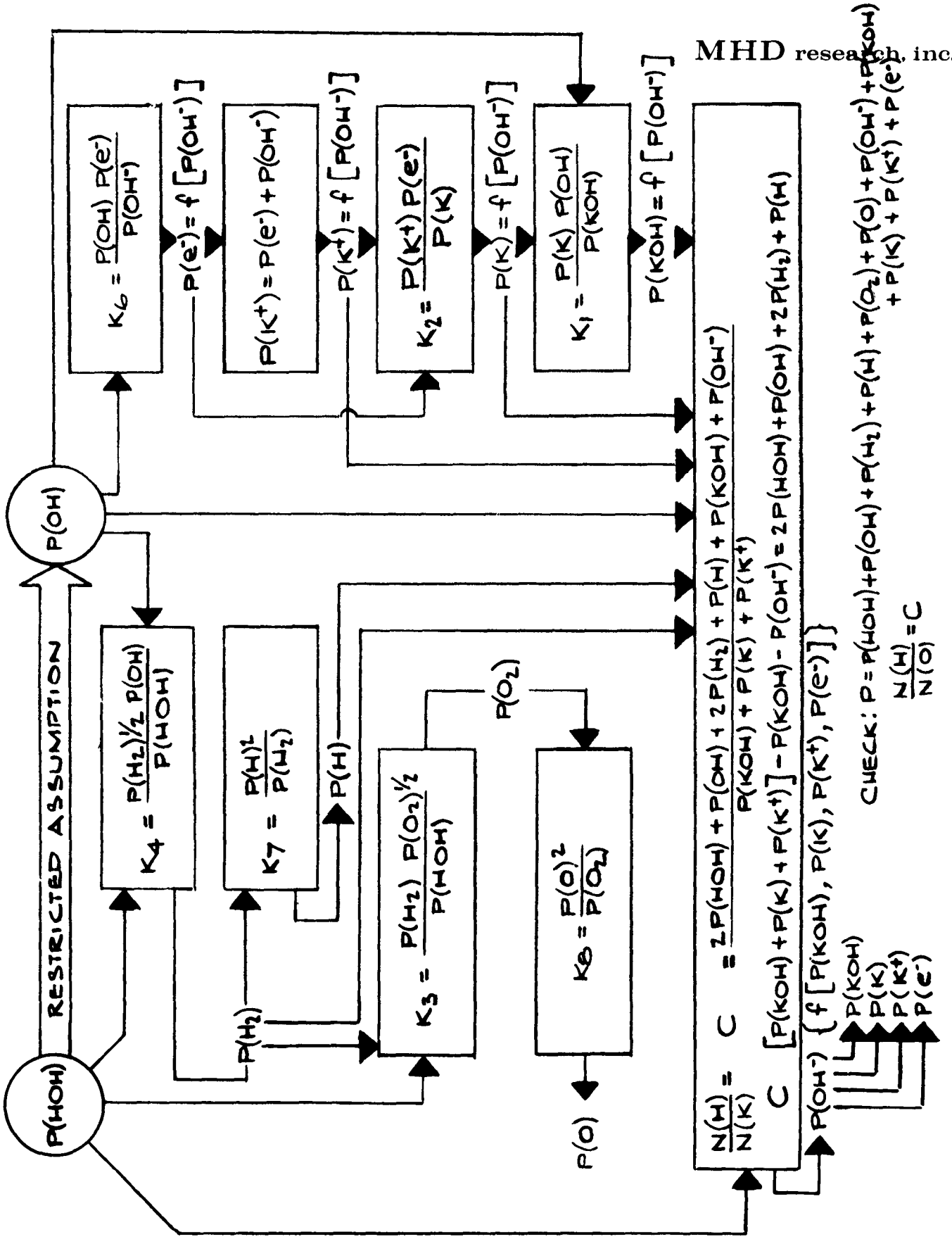

Figure 4.1 Flow chart showing method used for solution of simultaneous equations for reaction components.

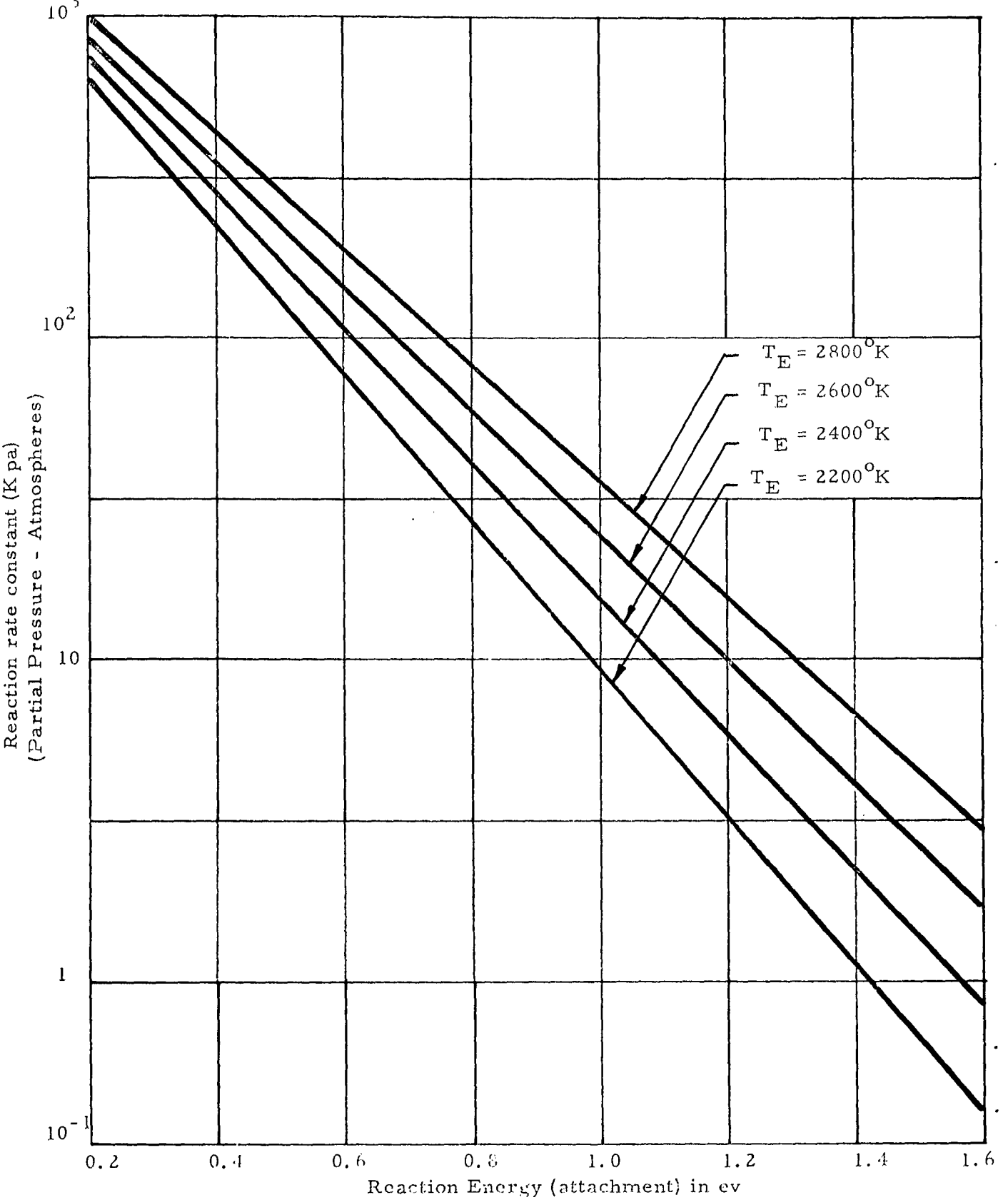

Figure 4.2 Reaction rate constant (K pa) as a function of reaction energy at various equilibrium temperatures for OH attachment

$$OH + e^- \rightleftharpoons OH^-$$

for some reason greatly exaggerated by the machine calculation. Specifically, the present results indicate that the concentration of potassium ions is approximately equal to the concentration of free electrons, and that the number of potassium ions is much less than the number of potassium atoms. The calculations also confirm the fact that the partial pressure of the hydroxyl negative ion is much less than the partial pressure of the free electrons. These results are in distinct and significant contradiction to the machine-calculated results. The physical consequences imply a return to the conventional concept of electronic dominance of plasma conductivity, rather than the ionic model previously advocated.

Direct comparison of the results presented here with published data is not easy, because most previous calculations have been carried out for the seeded hydrocarbon-oxygen systems that are commonly used for MHD power generation. In addition to the carbon compounds considered in such calculations, but not here, the seeding percentage rarely happens to coincide with the 1% by weight we assumed. However, certain relatively rough considerations show the general consistency of our results with those presented by Frost[8], chosen as an example. In effect, our more detailed calculations tend to confirm the validity of the results of the more approximate techniques Frost used.

Specifically, Frost's presentation of the dependence of electron density on temperature indicates, for potassium seed, that the density increases by approximately a factor 10 over the temperature range 2400^{o} - 2800^{o}K; our table indicates a similar increase.

Similarly, Frost treats the decrease in conductivity due to electron attachment (our Reaction 6, shifting to the left) and to KOH formation (Reaction 1, also to the left) by an approximate method, based on the Saha equation, which ignores "buffering" - interactions with other equilibria. His results are presented as factors (less than one) by which the conductivity obtained without consideration of OH attachment and chemical combination with alkali seed is decreased. Using our results on

concentrations to obtain parallel multiplicative factors, we obtain the comparisons:

Cause of Conductivity Reduction	Temperature	Frost's Factor	Our Factor
OH^- formation	2400°K	0.85	0.90
	2800°K	0.88	0.87
KOH formation	2400°K	0.62	0.60
	2800°K	0.85	0.83

Although the quantitative agreement is excellent (again tending to validate Frost's approximations), it is interesting to note that the trend of conductivity reduction due to electron attachment, as a function of temperature, is opposite for the two calculations. This is presumably due to the fact that the buffering interaction was not considered by Frost. One must conclude that calculations of electron attachment should take into account the effects of all species in the flow, including the buffering reactions, but that for practical purposes their neglect does not cause large errors.

4.3 Microwave Probing of Seeded Combustion Product Plasmas

4.3.1 Theory. The high frequency conductivity of partially ionized atmospheric pressure plasmas can be determined from the attenuation of microwave signals. If an attenuation of B nepers is measured when passing a test signal of angular frequency ω through the plasma, a distance of Z cm, the attenuation constant β is given for cases of interest ($n_e < 10^{12}, \omega > 10^{10}$), by the following relation:

$$\beta = \frac{B}{Z} = \frac{\sigma}{2c\epsilon_o} = \frac{n e^2 g}{2c\epsilon_o m(\omega^2 + g^2)} \quad .$$

$$= \frac{\sigma_{dc}}{2c\epsilon_o(1 + \omega^2/g^2)} \quad ,$$

where

- c = velocity of light ,
- ϵ_o = permittivity of free space ,
- n = charge carrier density (cm^{-3}) ,
- e = the electronic charge ,
- m = the charge carrier mass ,
- ω = $2\pi f$ = test angular frequency ,
- g = collision frequency for momentum transfer of charge carriers.

For electronic conductivity the charge carriers are electrons, and collision frequency g is approximately 3×10^{11} sec^{-1} in combustion product gases. For ionic conductivity, the charge carriers are positive and negative ions. The ionic collision frequency is lower than the electronic collision

frequency by approximately the square root of the mass ratio, which is approximately a factor of 200. Therefore, if the attenuation is measured at two frequencies, ω_1 and ω_2, which are chosen so that either ω_1 or ω_2, or both, are higher than the ion collision frequency, then one can solve the two simultaneous equations;

$$\beta_1 = \frac{neg}{2c\epsilon_o m(\omega_1^2 + g^2)},$$

$$\beta_2 = \frac{neg}{2c\epsilon_o m(\omega_2^2 + g^2)},$$

for n and g. Correspondingly, one can tell by the ratio of attenuations at the two frequencies whether ionic conduction or electronic conduction is the dominant process. In the case of pure ionic conduction, with millimeter wave signals, such that $\omega >> g_{ion}$, then the ratio of attenuations at two frequencies would be

$$\frac{\beta_1}{\beta_2} = \frac{\omega_2^2}{\omega_1^2}$$

For a typical case where β is measured at 9 KMC and 36 KMC, the attenuation should differ by a factor of 16.

For a more detailed look at attenuation in the case of electronic conduction, Figure 3.3 is a plot of attenuation versus electron density for a collision frequency of 2×10^{11} sec^{-1} for test frequencies of 9 and 35 KMC. In a typical case at 10^{11} electrons/cm^3, the attenuation at the two frequencies differs by a factor of 2.3.

4.3.2 Details of the Experimental Apparatus. These experiments were carried out in the combustion product flow facility described in Reference (1). Figure 4.3 shows the details of this facility. Figure 4.4 is a close-up photograph showing the external details of the test section and indicating the location of the microwave cavity. RG/96U waveguide for 35 KMC measurements is shown. Standard gain horns have been machined out of the interior of a water-cooled copper block, shown in Figure 3.2 in the previous section. The horns are loaded with boron nitride which is machined so as to fit back into the rectangular waveguide section with a tapered transition, to reduce the standing wave ratio.

For these experiments, the combustion products were derived from the combustion of ethyl alcohol (C_2H_5OH), and gaseous oxygen. The flow was seeded with 1/6% by weight of potassium, introduced as KOH dissolved in the ethyl alcohol. To lower the gas temperature, provision was made for the introduction of gaseous nitrogen as a diluent. Gas temperatures were determined by potassium resonance line reversal methods. The water-cooled calorimeter installed below the microwave cavity made it possible to continuously monitor gas temperature between optical readings.

During these experiments, it was determined that the power supply used to provide current for the black body tungsten strip lamp, used in the line reversal measurements, had an appreciable alternating current ripple which was not recorded on the direct current meter. This meant that a larger current was flowing in the lamp for a given current reading. The lamp had been calibrated in terms of brightness temperature versus current. The net effect was that in the operating range used for the combustion product experiments, the actual lamp temperature was about 160°K higher than had been previously believed. One major consequence of this change in calibration is to shift the conductivity

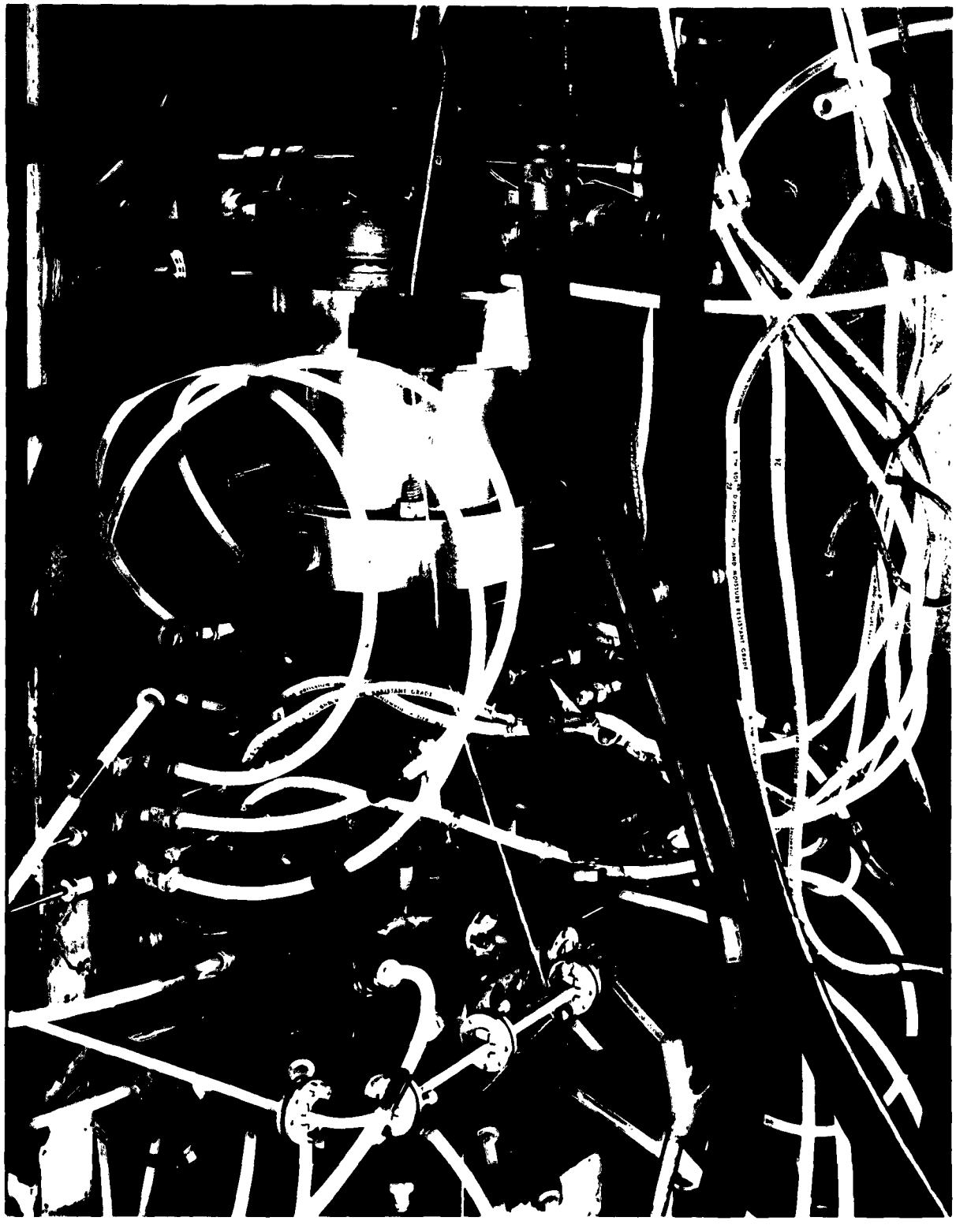

Fig. 4.4 Combustion Product Flow Facility
Experimental Details

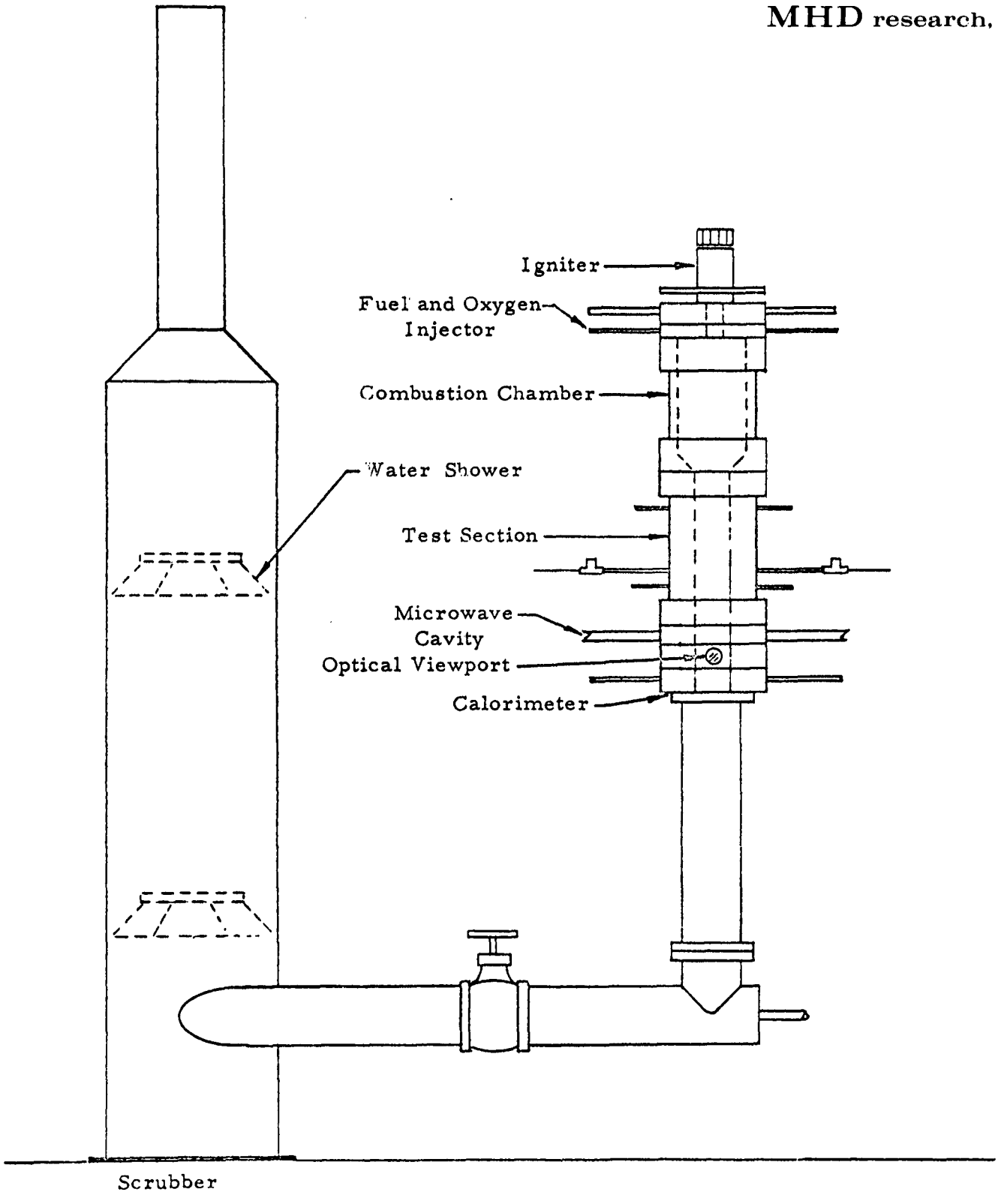

FIGURE 4.3

General Schematic of Conductivity Test Facility

measurements reported in Reference (1) for 1% potassium, to about 2600°K. The measured conductivity of approximately 9 mhos/meter from the linear at this temperature is then in excellent agreement with measurements reported by Brogan, et al [9], and others.[10] [11]

As previously stated, attenuation measurements were made at 9 KMC and 35.5 KMC. For a gas temperature of approximately 2400°K, the attenuation at 9 KMC was 1.45 nepers/cm, (12.6 db/cm), while the attenuation at 35.5 KMC was 0.592 nepers/cm. These two attenuation values can be used to find an effective collision frequency of 1.8×10^{11} sec^{-1}, which leads to an effective collision cross-section of 1.93×10^{-15} cm^2 for combustion products. This value is somewhat lower, by a factor of three, than the values derived from the electrical conductivity experiments. Several reasons can be advanced for disagreement between the two determinations. The microwave experiments, in general, do not have the electrode drops associated with the normal conductivity measurements derived from voltage current curves. Therefore the electrodeless methods should tend toward higher conductivity values, or lower cross-sections for a given gas temperature. Regardless of any comments as to the applicability of the microwave techniques, or their interpretation, these measurements clearly indicate that the electrical conductivity is primarily due to conduction by free electrons, and not to conduction by ions as had been indicated by the computer program. Ionic conductivity would have been indicated by a collision frequency of the order of 10^9 sec^{-1}.

APPENDIX A

Scaling and Geometry Considerations of Explosive-Driven MHD Generators

P. R. Smy* and C. N. McKinnon

Results to date (December 1962) on the shaped charge-driven pulsed MHD generator indicate that high power outputs will be obtained when the device is scaled to a larger size. Already 800 KW (lasting about 5 μ secs) have been delivered from a volume less than one cubic inch. The questions one may ask then, are:

1. What scaling factors apply to get an output of say 10^9 watts and higher?
2. If such a power output is possible, can the device compete (or compare) with capacitor storage or some other form of conversion?
3. How can the power be delivered for times longer than tens of μ secs, so more total energy is delivered to a load?
4. What form might such a high-powered device take?

Before considering the scale-up of an MHD generator, the proper perspective can be gained by looking at existing (competing) methods for generation of high power pulses.

The most obvious competitor is the capacitor bank. A typical capacitor bank occupying a total volume of 1 cubic meter might possess a

*Consultant, permanent address Department of Physics, University of British Columbia.

stored energy of 2×10^4 joules and provide a peak power of 10^{10} watts. Power supplies and switching equipment would of course take up more space. One drawback of this system is that, although a capacitor bank discharge can be initiated within fractions of a microsecond of a given instant, the capacitors must be charged prior to discharge. It is possible that capacitors could be maintained in the charged condition indefinitely, but even in this case the inevitable leakage current would require a substantial supply of electrical power to the bank. In this respect, capacitors are storage devices and not independent energy sources. The properties of compactness and low power consumption in the "primed" state make an explosive-driven generator an attractive proposition compared to capacitors. A very large amount of chemical energy is stored in a very small volume of explosive and no power is required to maintain the explosive in its "primed" state apart from the power consumed by the triggering device. Neglected here is magnetic field energy requirements as these could feasibly be supplied by permanent magnets. The problem is to convert this explosive energy into electrical energy.

Another competitor in the generation of pulse power are the new piezoelectric materials, which transform a direct mechanical stress into high voltage electrical power. The piezoelectric energy output that can be expected from a cubic meter is about 3×10^4 joules, which could be delivered in about 10^{-3} secs for a power output of the order of 10^7 watts. The problem is in providing the mechanical pressure of 15,000 psi over the desired surfaces. Again, explosive energy may be capable of providing the quick mechanical stress necessary for high power pulse generation.

1. Scaling

When designing a pulsed power generator it is necessary to know those properties of the generator which must be optimized. For

most applications it seems that the desirable properties are high power, high energy, compactness, and in certain instances low or zero power consumption in the "primed" condition. These properties are of course desirable in a continuous generator, but it should be noted that efficiency, a property essential in a continuous generator, has been omitted. It is this omission that lends a certain flexibility to the design of a pulsed MHD generator.

In the present approach, the explosion products are channeled through an MHD generator to provide a peak power of approximately 1 MW for a period of about five microseconds. The volume of the generator itself is about 10 cm^3. Properties of the gas in the region of interaction with the magnetic field calculated from experimentally determined quantities are:

$$\text{Velocity} \quad u \simeq 5 \times 10^3 \text{ m/sec},$$

$$\text{Electrical conductivity} \quad \sigma \simeq 2 \times 10^3 \text{ mho/m}.$$

The Rankine-Hugoniot equations imply a minimum gas density of about 5 kg/m^3.

With these experimental results, it is possible to estimate the power output from a generator with the much larger dimensions of 1 meter x 1 meter x 1 meter, and so compare the generator performance directly with the capacitor bank described above.

In an MHD generator in which the magnetic field strength is B, the power output per unit volume is:

$$P_{vol} = \frac{\sigma u^2 B^2}{4}.$$

Thus with the experimental values for σ, u, and with B equal to 1 weber/m^2 (feasible for permanent magnets), the resulting power density is about 10^{10} watts/m^3. Unfortunately, although this power output density is obtained with the present generator, it is unlikely that P_{vol} could have

such a high value with the much larger generator. There are two reasons for this:

1. At present the region of conducting gas is located within 4 cms of the shock front and thus (for strict scaling) only a small fraction (4%) of the total generator volume (1 meter x 1 meter x 1 meter) will be effective in power production at any given time. Of course it can be expected that this rather limited region of high conductivity might be extended by further experimentation with seeded materials and by use of large explosive charges.

2. As the dimensions of the generator are increased, the appropriate magnetic Reynolds number (R_m) becomes much greater than unity ,

$$R_m = \mu_o \sigma L u \quad .$$

In this equation μ_o is the permeability of the conducting medium (usually taken as the free space value) and L is a length characteristic of the interaction region. When R_m is greater than unity, the induced (generated) current perturbs the applied field[12] and places an upper limit on the power output of the generator of

$$P_{max} = \frac{2B^2 A u}{\mu_o} \quad ,$$

where A is the flow cross-section.

The upper limit imposed here is a result of the generator design, and does not take into account the possibility of recovering inductively energy extracted from the gas system and stored magnetically. The usual "low" R_m relationship

$$P \cong \sigma u^2 B^2$$

no longer applies.

The conditions for the present generator are:

$$L \cong 2 \times 10^{-2} \text{ meters}$$

$$R_m \cong 0.12 \ .$$

Therefore, the expected output power density should be 2×10^{10} watts/m^3. For the generator with L equal to one meter, R_m has a value of six, and so the appropriate generator power density is more accurately given by the high relationship. Therefore,

$$P_{max} \ (L = 1 \text{ meter}) = 8 \times 10^9 \text{ watts.}$$

This is somewhat less, but on the same order, as that given by the low R_m relationship. Another very similar effect which also becomes important if R_m is much greater than unity, is the internal inductance of the generator. It can be shown that the power output from the generator will be substantially inhibited for the time it takes the gas shock front to transverse the generator due to this inductive effect.

It can be seen that on the basis of either of the above mechanisms, the power output density will decrease with increasing generator volume. However, a one cubic meter generator would still produce respectable

quantities of power and energy:

$$P \simeq 10^9 \text{ watts}$$

$$E \simeq 2 \times 10^5 \text{ joules.}$$

This is more than competitive with other pulse power sources.

If low electrical power consumption prior to triggering is not a prime consideration, then electromagnets could be used (rather than permanent magnets); this would boost the applied field strength up to say 5 webers/m^2 and so boost the power and energy output by a factor of 25. In any event, the source of magnetic field would occupy a substantial volume and would probably increase the total size of the power source by a large factor with the results that an MHD generator and condenser bank both capable of delivering between 10^5 and 10^6 joules would both occupy much the same volume.

If in some way the extent of the conducting region could be increased to fill all of the generator then the power output at 5 webers/m^2 would be about 2×10^{11} watts, and this power would be available for the duration of flow of the conducting gas. It would seem to be well worthwhile to continue investigation of seeded explosions. Measurements already obtained show that the velocity of the exploding gases past a given point remain more or less constant for 50 to 100 microseconds which is ten times the duration for which the conductivity remains high. This fact, together with other considerations, indicates that the fall-off in conductivity is either due to cooling of the explosion gases or insufficient seeding content. The latter question will probably be answered in the present program. The former mechanism should be fairly easy to calculate. Conduction and diffusion effects will be very small at these high densities and the main heat loss will probably be due to continuum radiation.[13] The experimental conditions here may be rather different from those used by previous workers in that, with these high gas densities, it is possible that the radiating plasma is optically thick. Incidentially, from this point of view, a 1 cubic

3. The problem of scaling such a generator is not simple because of the unusually high velocities and conductivities generated by seeded explosives, with the result that generators of modest size produce a high R_m interaction in which the usual low R_m generator relations do not apply.

2. Proposed Radial MHD Generators

From the above discussion it seems that the explosive driven rectangular MHD generator is a relatively inefficient device when readily attainable magnetic field strengths are used, the reason being that the dynamic pressure, ρu^2, of the incident flow is much greater than the available magnetic pressure,

$$\frac{(2B_o)^2}{2\mu_o} .$$

Also it appears that most of the explosive energy is wasted in inelastic expansion of the explosion chamber due to the small solid angle that the generator subtends at explosive. Even optimum charge shaping results in no more than 5% of the chemical energy converted into directed motion in the MHD channel.

A notable improvement in both respects can be achieved by using a cylindrical configuration in which a stick of explosive explodes radially. In this case the density of the exploding gas must perforce decrease with with increasing radius to provide a more efficient match between the dynamic and magnetic pressures and also ensure a much greater interaction cross-section. The two types of radial MHD interaction are adaptions of the well-known Θ and Z pinch discharges.

meter generator might well provide a more extended region of high conduction than the present generator.

So far no attempt has been made to relate the power output to the power input although it has been assumed that little retardation of the flow velocity occurs in the generator. The power input into the generator is taken to be approximately equal to the kinetic energy flux:

$$P_{in} \cong 1/2 \rho u^3 A \quad .$$

If the following conditions apply:

$$\rho = 5 \text{ kg / meter}^3$$
$$u = 6 \times 10^3 \text{ m/sec}$$
$$A = 1 \text{ meter}^2$$

then

$$P_{in} \simeq 5 \times 10^{11} \text{ watts.}$$

Only in one case, that of high magnetic field strength (5 webers/m^2), and extended conductivity, would one expect any flow retardation since, in every other case, the input power is much greater than the output power.

In summary the main points in this section on the rectangular MHD generator are:

1. A large (1 cubic meter) generator would be comparable in many respects with a similar sized condenser bank, but would possess the advantage of low or zero power consumption in the "primed" state.

2. Such a device would be much more useful if some way is found in the present work of extending the conduction much further behind the shock front.

In these interactions, however, the initial radii of the plasma column would be small, i.e., that of the explosive, whereas the conventional gaseous discharges and initial radii are at their maximum values.

2.1 "θ-Pinch" MHD Device

This geometry would consist of a radial explosion in a region of axial field surrounded by a solenoid, (see Figure A.1). For simplicity we will consider the solenoid to be short circuited initially. With the solenoid short circuited, the total flux through the solenoid remains constant. To some extent the expanding radial explosion is diamagnetic and so the magnetic field will be compressed by the explosion into an annulus at the periphery of the coil. This compression of magnetic field lines corresponds to an increase in the magnetic energy of the system

$$\int_{vol} \frac{B^2}{2\mu_o} \, dv \ .$$

Much of this magnetic energy is readily convertible into electrical energy by switching a suitable external impedance into the solenoid circuit as the compression of field lines nears a maximum. The smallest volume of the annulus (if we assume negligible attenuation of radial explosion velocity) is determined by the velocity and conductivity distribution within the exploding column, and this limit is a consequence of the imperfect diamagnetism of the exploding column. This cross-section will be

$$\simeq \frac{2\pi r_o}{\mu_o \sigma \frac{dr}{dt}} \ .$$

It should be emphasized that this is a very approximate relation. It should be fairly simple to obtain a much more accurate relation for a

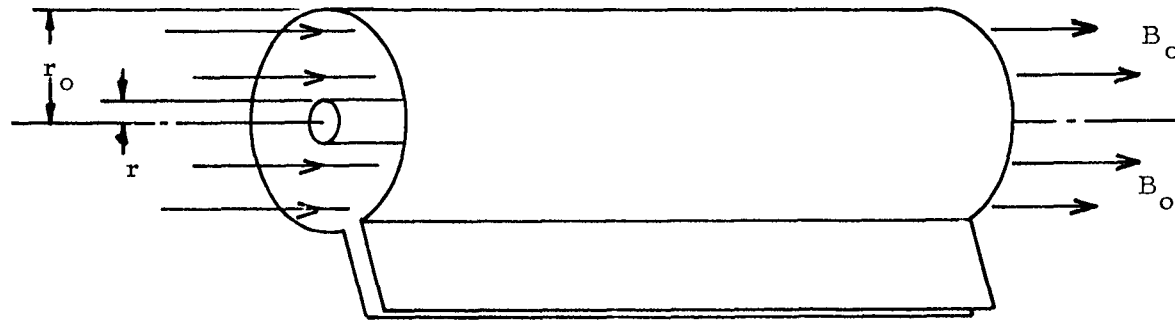

Before Ignition

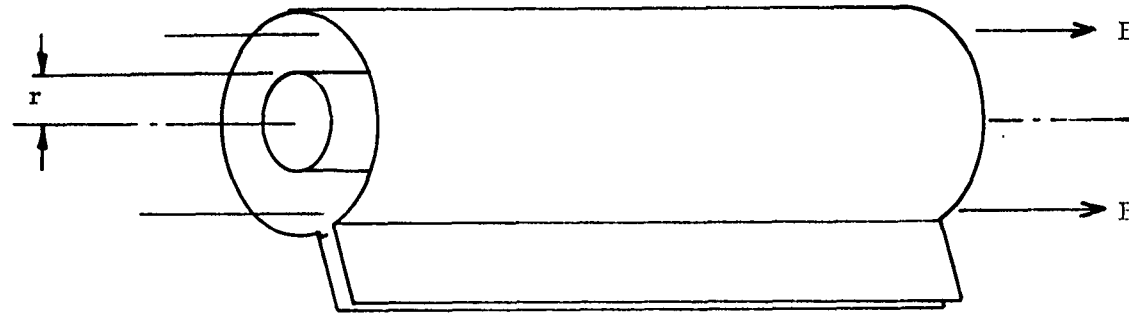

After Ignition

Figure A.1 "Θ-Pinch" MHD Generator

simple model, but this has not been attempted since the actual physical properties of the system are not well known. Assuming the above relation is correct, we can work out the enhanced magnetic energy of the system. If the inital field is B_o and the solenoid radius is r_o, then applying flux conservation we have

$$B = \frac{\mu_o \sigma \frac{dr}{dt} B_o r_o}{2}$$

and so the final magnetic energy is,

$$\frac{\mu_o \sigma \frac{dr}{dt} l}{2} \left(\frac{B^2}{2\mu_o}\right) \approx \frac{R_m}{2} \text{ x original magnetic energy.}$$

Taking A = 1 meter^2, l = 1 meter, B_o = 1 weber/meter^2, and $R_m \simeq 6$, we have a final magnetic energy (E_m) of 1 M joule.

Most of this magnetic energy could be converted by electrical energy in a time : $\tau = \frac{1}{u^2 \sigma \mu_o} \tilde{=} 30$ μsecs.

This would correspond to a power of approximately 3×10^{10} watts.

While these figures are undoubtedly optimistic, it seems probable that both power and energy would be greater than one-tenth of the above values. This inductive removal of energy has several advantages. For example, it eliminates electrode sheath effects together with their associated power losses and by varying the number of turns of the solenoid, one can vary the output impedance to match a particular load.

2.2 "Z-Pinch" MHD Device

In the "Θ-pinch" device, only field strengths which could be obtained using permanent magnets were considered. In the "Z-pinch" device, see Figure A.2, the initial interacting magnetic field is generated

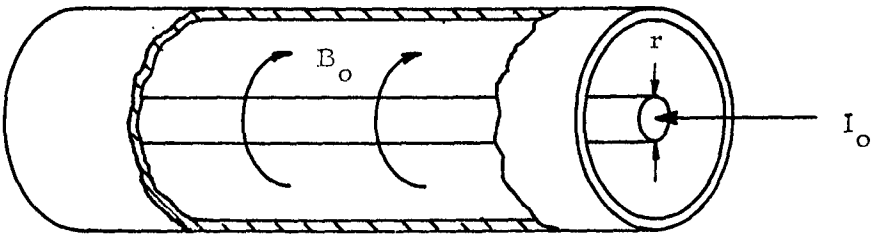

Before Ignition

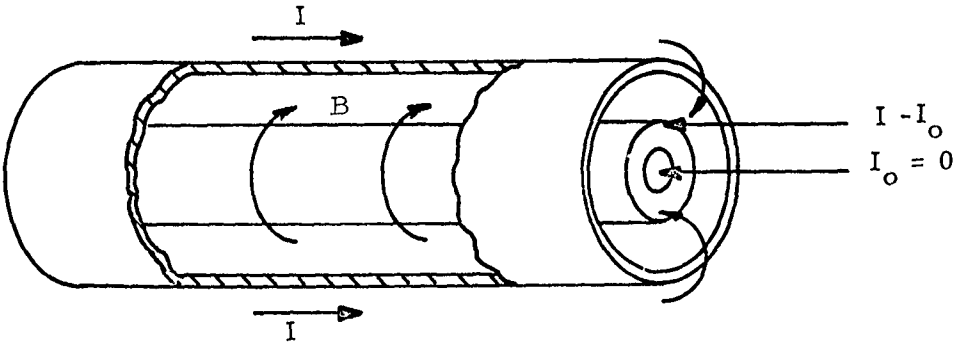

After Ignition

Figure A.2 "Z-Pinch" MHD Generator

by a current along the axis of the system, i.e., along the center of the cylinder of explosive. This might be achieved by pulsing current through a thin wire coated with explosive, vaporizing the wire and so detonating the explosive. The wire would be held between the center of two parallel metal electrodes with the return lead consisting of rods situated around the periphery of the device to form a coaxial assembly. The system effectively acts as a current amplifier; the aximuthal magnetic field and the radial velocity of the explosion produce an axial E field which augments the existing axial current and so strengthens the magnetic interaction. We will consider a radial explosion in which the exploding column increases in radius at a constant rate from an initial radius r_o, the conductivity of the exploding gas is constant, and the initial current is I_o. As before, we neglect magnetic retardation of the gas on the grounds that this can be eliminated by using sufficient explosive. If appreciable retardation does occur, then the conversion of a large fraction of the kinetic energy of the explosion into electrical energy has been achieved. For simplicity, consider the electrodes to be short circuited and calculate the enhanced magnetic energy of the system. If $\frac{B}{\mu_o}$ is the field at a point from the axis and I is the total current passing within this distance from the wire then,

$$B = \frac{2 I \mu_o}{r} .$$

If v is the radial velocity at any point (the assumption of constant uniform velocity is made for theoretical simplicity; it is virtually certain this would not apply in practice), then the induced electric field at a point from the axis is

$$E = \frac{v \times 2 I \mu_o}{r} ,$$

and so the total current

$$I = I_o e^{\sigma \mu_o v (r - r_o)}$$

$$= I_o e^{R_m}$$

With a system whose dimension L equals 1/2 m, and R_m equals 3, it is seen that considerable current and hence electrical energy amplification might be obtained. Here again the power output might be inhibited to some extent by the self-inductance of the generator for the useful case of R_m much greater than one. This system is very sensitive to R_m. For example, if σ equals 5×10^3 mhos/meter, then

$$\frac{I}{I_o} = e^{15} \text{ rather than } e^3 .$$

2.3 Multi-State Power Generation

Both of the preceding geometries are attempts to get high power outputs by using the explosive energy to: (1) generate a high strength magnetic field, and (2) use the interaction of the field generated and conducting fluid to produce a high net electrical power.

The process of generating a high magnetic field using explosives has already been demonstrated.[14] In this case magnetic flux is generated inside a one-turn (cylindrical) solenoid by a condenser discharge. Detonating explosive charges surround the cylinder, and upon implosion collapse the cylinder, trapping the flux inside. Fields as high as 3 megagauss (300 webers/m^2) over a volume of several cm^3 have been recorded. In fact, the imploding cylinder generated such a high magnetic pressure ($P = \frac{B^2}{2\mu_o}$) that "turnaround" of the cylinder was noticed.

What this means is that perhaps instead of using one device for both steps above, separation of function may yield a more powerful (albeit more complicated) device. Since overall conversion efficiency

may not be the important parameter, the use of explosives in one stage to generate the magnetic field in a second stage which uses explosives to generate ionized gas, may yield a significant increase in the interaction and hence power output.

2.4 Significance of R_m in these Configurations

There are basically two types of power extractions described in the foregoing devices. In the cartesian MHD generators which have been described, energy is hopefully extracted at the same rate that it is converted from kinetic to electric energy. It is this feature that allows an expression of maximum power output to be derived. In the radial configurations, the kinetic energy of the stream is first stored magnetically and then recovered by inductive methods. Thus, the peak power output of such a system is regulated by the recovery method, and not by the energy flux of the stream or the initial volume energy content of the magnetic field. The value of R_m determines to a large degree, the effectiveness of the magnetic storage type of device because as

$$R_m \rightarrow \infty ,$$

this type of device becomes efficient. Increasing R_m beyond a certain limit would be of little value in the cartesian generator with direct extraction. However, if inductive removal of energy is utilized with this geometry, it can be generally stated that optimum operation of MHD generators will occur at the highest possible R_m.

We have frequently taken the applied field strength to be 1 weber/m^2, i.e., a field strength readily obtainable with permanent magnets. If we consider the use of the higher fields obtainable with electromagnets then the ratio -

$$\frac{\text{energy output}}{\text{initial magnetic energy}}$$

becomes a very significant parameter since in this case the initial magnetic energy can in any case be readily converted to electrical energy by switching off the magnetizing current.

If field strengths greater than 1 weber/m^2 are required in the above radial generators, it follows that R_m must be appreciably greater than unity for the generators to be practical.

Both radial generators become efficient sources of power when their dimensions are increased to about 1 meter; however, it is necessary that all the exploding gas be highly conducting rather than a region of a few cms thickness as at present.

2.5 Use of a Copper Piston

One way of increasing the effective R_m of the system would be to introduce a copper piston into the system. The much higher conductivity of copper would ensure a relatively powerful magnetic interaction even though the maximum achievable velocity of the piston ($\sim 10^3$ m/sec) would be somewhat less than the gas velocities we have been considering.

Two copper piston generators are proposed:

(1) The first generator is a solid, explosion-driven copper slug injected along the axis of a solenoid in which there is an initial axial field. This system would work in much the same manner as the "θ-pinch" device considered previously. Calculations indicate that with an applied field of 1 weber/m^2, a generator of 1 liter in volume might provide an energy output of approximately 10^4 joules at 10 MW. This is a very respectable energy output for a small volume. Energy would appear to scale as dimension to the 5/2ths power although joule heating of the surface of the copper slug might prove a problem at very large dimensions.

(2) The second generator is a radial explosion which moves a thin (a few mm) annular copper cylinder outward towards the inner surface of a surrounding solenoid. The important parameters here are: (a) the dimensions of the copper annulus, (b) it must stay in one piece during the expansion, (c) it must be effectively diamagnetic for the duration of the expansion, and (d) it must be thin enough to achieve a substantial radial velocity. These requirements may be mutually incompatible.

REFERENCES

(1) Jones, M. S., Rockman, C. H., Hellund, E. J., McKinnon, C. H., and Blackman, V. H., "The Physics of MHD Channels", final report, Contract Nonr 3523(00), MHD Research, Inc., Newport Beach, California, July 1962.

(2) Nagamatsu, H. T., Sheer, R. E., and Weil, J. A., "Non-Linear Electrical Conductivity of Plasma for Magnetohydrodynamic Power Generation", ARS Paper 2632-62, Space Power Systems Conference, Santa Monica, California, September 1962.

(3) Friedman, et al, "Study of Electron Generation by Solid Propellant Techniques", Atlantic Research Corporation, Alexandria, Virginia, September 21, 1962.

(4) Sherman, A., "A High Performance, Short Time Duration, MHD Generator System", ARS Paper No. 2558-62, Space Power Systems Conference, Santa Monica, California, September 1962.

(5) Hord, R. A., and Pennington, J. B., "Temperature and Composition of a Plasma Obtained by Seeding a Cyanogen-Oxygen Flame with Cesium", NASA TN D-380, May 1960.

(6) Basu, S., "Ionization in Seeded Detonation Waves", Phys. Fluids 3, No. 3, June 1960, p 456.

(7) Sutton, G. P., "Rocket Propulsion Elements", Wiley and Sons, New York, 1956.

(8) Frost, L. S., "Conductivity of Seeded Atmospheric Pressure Plasmas", JAP, 32, 2029, No. 10, October 1961.

(9) Brogan, T. R., et al, "A Review of Recent MHD Generator Work at the AVCO-Everett Research Laboratory", Third Symposium on the Engineering Aspects of Magnetohydrodynamics, Rochester, New York, March 1962.

(10) Devime, R., Lecroart, H., X. N'Guyen Duc, Poncelet, J., and Ricateay, P., "Conductivity Measurements in Seeded Combustion Gases", Paper No. 32, Symposium on Magnetoplasmadynamic Electrical Power Generation, Newcastle upon Tyne, September 1962.

(11) Zimin, E. P. and Popov, A. V., "Research on the Electrical Conductivity of Combustion Products with Potassium Seeding", Paper No. 21, Symposium on Magnetoplasmadynamic Electrical Power Generation, Newcastle upon Tyne, September 1962.

REFERENCES (Cont'd.)

(12) Pain, H. J., and Smy, P. R., "Experiments on Power Generation from a Moving Plasma", Journal of Fluid Mechanics, 11, 51, February 1961.

(13) Lin, S. C., Resler, E. L., and Kantrowitz, A., "Electrical Conductivity of Highly Ionized Argon Produced by Shock Waves", J. App. Phys. 26, 95, No. 1, January 1955.

(14) Fowler, C. M., et al, "Flux Concentration by Implosion", p 269, Proceedings of the International Conference on High Magnetic Fields, 1961, Edited by H. Kohm, et al, John Wiley, New York, 1962.

DISTRIBUTION LIST

	No. Copies
Director, Advanced Research Projects Agency The Pentagon Washington 25, D. C. Attn: Dr. John Huth	2
Office of Naval Research Power Branch (Code 429) Washington 25, D. C. Attn: Mr. John A. Satkowski	6
Office of Naval Research 1030 East Green Street Pasadena, California Attn: Mr. Russell Lathrop	1
U. S. Naval Research Laboratory Washington 25, D. C. Attn: Dr. Alan Kolb, Code 7470 Mr. B. J. Wilson, Code 5230 Technical Information Division	 1 1 6
Aeronautical Systems Division, AFSC Wright-Patterson AFB, Ohio Attn: Mr. Don Warnock (ASRMFP-2) Dr. J. Sirons	 1 1
Aeronautical Systems Division, AFSC Weapons Lab, Eglin AFB, Florida Attn: Mr. Robert Cross (ASQW)	1
Air Force Office of Scientific Research Washington 25, D. C. Attn: Dr. Milton M. Slawsky	1
U. S. Naval Ordnance Test Station China Lake, California Attn: Dr. H. Powell Jenkins, Jr. Dr. Dean Mallory	 1 1

Rome Air Development Center
Rome, New York
Attn: Mr. Frank J. Mellura 1

U. S. Naval Ordnance Laboratory
NA Division
White Oak, Maryland
Attn: Mr. Wallace Knutsen 1
Library 1

Armed Services Technical Information Agency
Arlington Hall Station
Arlington 12, Virginia 10

U. S. Army Research & Development Laboratory
Fort Belvoir, Virginia
Attn: Mr. Frank Shields (ERD-EP) 1

NASA Lewis Research Center
21000 Brookpark Road
Cleveland 35, Ohio
Attn: Mr. Wolfgang Moeckel 1
Mr. J. Howard Childs 1

U. S. Atomic Energy Commission
Division of Reactor Development
Direct Energy Conversion Section, RD:AED
Germantown, Maryland 1

Dr. J. E. McCune
Aeronautical Research Associates of Princeton
Princeton, New Jersey 1

Dr. T. Brogan
AVCO Everett Research Laboratory
2385 Revere Beach Parkway
Everett, Massachusetts 1

Dr. J. Cole
Department of Aeronautics
California Institute of Technology
Pasadena, California 1

Mr. Arthur Sherman
General Electric - Valley Forge
Valley Forge Space Technical Center
Philadelphia 1, Pennsylvania 1

Dr. George Sutton
General Electric - Valley Forge
Valley Forge Space Technical Center
Philadelphia 1, Pennsylvania 1

Dr. M. Talaat
Martin Marietta Corporation
Nuclear Division
Baltimore 3, Maryland 1

Prof. H. H. Woodson
Electrical Engineering Department
Massachusetts Institute of Technology
Cambridge 39, Massachusetts 1

Dr. B. C. Lindley
Nuclear Research Centre
C. A. Parsons & Co., Ltd.
Fossway, Newcastle upon Tyne 6, England 1

Dr. W. O. Carlson
Radio Corporation of America
Defense Electronic Products
Moorestown, New Jersey 1

Dr. Robert Eustis
Thermosciences Division
Stanford University
Stanford, California 1

Mr. W. C. Davis
TRW-TAPCO Group
7209 Platt Ave.
Cleveland 4, Ohio 1

Mr. Stan Markowski
Pratt & Whitney Aircraft
400 Main Street
East Hartford 8, Connecticut 1

Mr. D. T. Swift-Hook
Central Electricity Research Laboratories
Cleeve Road, Leatherhead, Surrey, England 1

Dr. Richard Schamberg
Rand Corporation
1700 S. Main Street
Santa Monica, California 1

Dr. Sam Naiditch
Unified Science Associates
826 Arroyo Parkway
Pasadena, California 1

Dr. Peter Smy
Physics Department
University of British Columbia
Vancover, B.C., Canada